DNA barcoding reveals ongoing immunoediting of clonal cancer populations during metastatic progression and in response to immunotherapy

Louise A. Baldwin[1,2], Nenad Bartonicek[1,2], Jessica Yang[1], Sunny Z. Wu[1,2], Niantao Deng[1,2], Daniel L. Roden[1,2], Chia-Ling Chan[1], Ghamdan Al-Eryani[1,2], Alexander Swarbrick[1,2], and Simon Junankar[1,2*].

Affiliations

(1) The Kinghorn Cancer Centre and Cancer Research Theme, Garvan Institute of Medical Research, Darlinghurst, NSW 2010, Australia

(2) St Vincent's Clinical School, Faculty of Medicine, UNSW Sydney, NSW 2052, Australia

*Corresponding author: s.junankar@garvan.org.au

Key words: Immunoediting, immunotherapy resistance, breast cancer

Abstract

Cancers evade the immune system in order to grow or metastasise through the process of cancer immunoediting. While checkpoint inhibitor therapy has been effective for reactivating tumour immunity in some cancers, many solid cancers, including breast cancer, remain largely non-responsive. Understanding the way non-responsive cancers evolve to evade immunity, what resistance pathways are activated and whether this occurs at the clonal level will improve immunotherapeutic design. We tracked cancer cell clones during the immunoediting process and determined clonal transcriptional profiles that allow immune evasion in murine mammary tumour growth in response to immunotherapy with anti-PD1 and anti-CTLA4. Clonal diversity was significantly restricted by immunotherapy treatment at both the primary and metastatic sites. These findings demonstrate that immunoediting selects for pre-existing breast cancer cell populations, that immunoediting is not a static process and is ongoing during metastasis and immunotherapy treatment. Isolation of immunotherapy resistant clones revealed unique and overlapping transcriptional signatures. The overlapping gene signature was predictive of poor survival in basal-like breast cancer patient cohorts. Some of these overlapping genes have existing small molecules which can be used to potentially improve immunotherapy response.

Introduction

All cancers must find ways to evade the immune system so that they can continue to grow (*1*). Previous studies have established that this occurs through a process called immunoediting (*2*). During immunoediting, the more immunogenic cancer cells are selectively eliminated by the immune system thus leaving behind less immunogenic cancer cells that are then free to expand. Immunoediting can occur through multiple mechanisms, these include the elimination of cells with strong immunogenic mutations, leading to the loss of neo-antigens (*3*) or the selection of cells with elevated expression of various immunosuppressive programs (*4*).

Immunotherapies look to overcome some of the immune evasion pathways established by the cancer cells to avoid recognition and elimination by the immune system during immunoediting. The prominent clinically approved immunotherapies for solid tumours target T cell checkpoint molecules (eg. anti-

CTLA-4 and anti-PD1) to overcome T cell exhaustion (*5, 6*). In select cancer types such as melanoma, these drugs have dramatic effects in a large proportion of patients (*7*). Unfortunately for metastatic breast cancer early clinical trials have seen few patients experiencing durable responses even in the most sensitive basal-like subtype of breast cancer (*8*). This indicates that in metastatic breast cancer, resistance can rapidly develop to anti-PD1/PDL1 therapy and suggests that alternate immune drug targets are needed for breast cancer.

While the immune system is known to play a role in breast cancer outcome (*9*) and recent evidence has indicated that immunoediting can occur in a transgenic mouse model of breast cancer (*10*), very little is known about the specifics of immune evasion by breast cancer cells. The majority of studies examining this phenomenon were performed in the highly mutated MCA carcinogen driven sarcoma model, and could not track the response at a clonal level (*11*). Of interest, a recent study suggested that immunoediting by T cells can occur at the clonal level, by demonstrating the selection of clones that contain less-immunogenic fluorophores (*12*). This leaves an important gap in our collective knowledge as to the mechanisms employed in less immunogenic tumours such as breast.

NK cells and T cells have both been demonstrated to play a role in immunoediting (*13, 14*). However, the majority of recent research has focussed on pathways relevant to T cell recognition (*15-19*). Downregulation of MHC is one mechanism by which cancer clones become impervious to T cells (*20*), but this inherently makes them targets of NK activity. In breast cancer NK dysfunction is noted and this is regulated by microenvironmental factors (*21*). Data on resistance pathways that allow for immune evasion from both T cells and NK cells are currently more limited.

To understand the process of immunoediting in breast cancer we conducted DNA barcoding (*22, 23*) of murine EMT6 and 4T1 mammary carcinoma cells, which were introduced into both immune competent and immunocompromised mice (Fig 1). DNA barcoding allows tracking of individual clones and clonal expansion while avoiding introduction of potentially immunogenic proteins (*24*). This system allowed us to analyse immunoediting *in vivo* at primary and metastatic sites and to study whether resistance to checkpoint immunotherapy developed from pre-existing or *de novo* generated cell populations. We show that immunoediting is initiated by the endogenous immune system in primary tumours and that cancer cells undergo a second round of immunoediting during metastasis. We further observed that immunoediting of specific clones is enhanced at both sites by checkpoint immunotherapy. We also identified cancer cell clones highly resistant to immunotherapy. RNA-sequencing (RNA-Seq) analysis of these resistant clones demonstrated that each clone had activated unique immune evasion pathways, with one downregulating MHC-I expression and another upregulating PD-L1. However, these clones also contained a common gene expression signature that is highly predictive of poor survival in both the METABRIC and TCGA basal-like breast cancer cohorts. This study has thus determined the patterns of immunoediting at a clonal level, that metastatic cells undergo a second round of immunoediting, and that immunotherapy significantly restricts clonal diversity. We go on to determine unique pathways activated in immune evasive cancer cells that are targetable and could improve immunotherapy response in breast cancer patients.

Results:

Immunoediting of breast cancer cells in the primary tumour

To understand the role of the immune system and immunotherapy in shaping the clonal dynamics of cancer cells within primary tumours we used the immunotherapy-sensitive syngeneic mammary carcinoma model EMT6 (*25*). The ClonTracer DNA barcode library (*22*) was introduced into the EMT6 cells resulting in ~41 000 unique barcodes identified by DNA sequencing. Following inoculation of 250 000 cells (~6 fold over representation of each barcode) into the mammary fat pad we compared the number of clones able to engraft and grow in immune-competent, syngeneic wild-type (WT) Balb/c mice or severely immunocompromised NOD SCID Gamma (NSG) mice (Fig 2A).

Tumour growth was much more rapid in the NSG mice with tumours reaching ethical endpoint on day 14 post-transplant, whereas wild-type mice all reached ethical endpoint by day 23 (Fig 2B). This led to NSG mice having significantly shorter overall survival (median survival 14 days) when compared to wild-type mice (median survival 22 days, Mantel-Cox p=0.009), demonstrating that the immune system plays an important role in controlling primary tumour growth in the EMT6 model (Fig 2C).

To examine the influence of immunotherapy on tumour growth & clonal dynamics, we compared wild-type mice treated with combination immunotherapy (anti-PD1 + anti-CTLA4) or control antibodies starting from day 10 when tumours were approximately 200mm^3 (Fig 2A). All control mice reached ethical endpoint by day 23 (Fig 2D). In contrast, all treated tumours regressed following treatment, with 50% relapsing and reaching ethical endpoint between days 46 and 54 (Fig 2D). The remaining immunotherapy treated mice remained tumour free when the experiment was terminated on day 60. Kaplan-Meier analysis demonstrated that immunotherapy significantly increased survival with median survival increasing from 22 days to 57 days (Mantel-Cox p=0.0006) (Fig 2E).

To determine if immune control of tumour growth was driven at a clonal level, we examined the number and distribution of barcodes present in primary tumours. We found that at ethical endpoint the tumours grown in NSG mice had over 50 times the number of unique barcodes as tumours grown in control WT mice (p=0.0002, unpaired t-test), which in turn had more than 20 times the number of unique barcodes found in immunotherapy treated WT mice (p=0.0019, unpaired t-test) (Fig 2F). We applied Shannon diversity analysis to these samples to understand how the immune system influenced the diversity of barcodes. Shannon diversity index is determined by how evenly distributed the barcodes are within a population and is only moderately influenced by barcode number. Analysis of barcode diversity revealed a trend to a reduction in barcode diversity in the tumours from the control Balb/c mice compared to the NSG mice, whereas there was a dramatic reduction in barcode diversity following immunotherapy treatment (p<0.001 unpaired t-test) when compared to the control treated mice (Fig 2G). This data indicates that a subset of EMT6 cells are more resistant to the endogenous immune system but that this selection does not skew the evenness of the barcode distribution dramatically. This suggests that the clones that are resistant to the immune system all have a similar level of resistance. In contrast immunotherapy applies a much more stringent bottleneck that only a limited

144 number of clones can readily overcome and with a high variability in the levels of
145 resistance. Further analysis identified specific EMT6 clones that were
146 reproducibly enriched across multiple replicate mice following immunotherapy
147 treatment indicating that they had a pre-existing resistance phenotype that was
148 being positively selected for (Fig 2H).

149 **Immunoediting of breast cancer cells during metastasis**

150 To determine whether immunoediting continued during metastatic dissemination
151 and whether specific metastatic clones were enriched or depleted, we turned to
152 the highly metastatic 4T1 mammary carcinoma model, as the EMT6 cell line is
153 poorly metastatic (*26*). The barcode library was introduced into the 4T1 cells
154 leading to a cell line with ~5000 unique barcodes. To see how the immune system
155 regulated clonal cancer growth during the metastatic cascade, 50,000 cells (a ~
156 10-fold over- representation of each barcode) were inoculated into the mammary
157 fat pad of WT and NGS mice. Primary tumours were resected 15 days following
158 inoculation to allow metastases to develop (Fig 3A). Following primary tumour
159 resection all mice developed lethal lung metastases. NSG mice succumbed to
160 metastatic disease earlier than WT mice with a median survival of 25.5 days verses
161 35 days (p = 0.0002, Mantel-Cox Log-rank test) (Fig 3B). Primary tumour size at
162 resection was equivalent between the groups (Sup Fig 1A). Adjuvant
163 immunotherapy with combination anti-PD1 + anti-CTLA4 led to a modest but
164 significant increase in survival (37.5 days) versus control treated mice (33 days;
165 p=0.0121, Mantel-Cox Log-rank test) (Fig 3C).

166 We then examined whether the endogenous immune system shaped metastatic
167 clonal dynamics. While primary tumours contained similar numbers of clones and
168 barcode diversity in NSG and WT hosts (Fig. 3D and Sup Fig 1B, C), metastatic
169 lungs of NSG mice contained ~3 times as many barcode clones as WT controls (Fig
170 3D). We next sought to determine if the increase in survival following
171 immunotherapy (Fig. 3C) was associated with alterations in clonal dynamics. As
172 the treatment was only given after excision of the primary tumour, the
173 immunotherapy would only affect the outgrowth of cancer cells that had already
174 metastasised to the lung. Despite only observing a modest increase in survival
175 following combination immunotherapy (Fig 3C), we observed a 70% reduction in
176 the number of clones able to form metastases (Fig 3E).

177 The increase in barcode number in the lungs of NSG mice was associated with a
178 significant increase in diversity as measured using the Shannon diversity index
179 (Fig 3F). This shows that the endogenous immune system restricts the number
180 and skews the diversity of metastatic clones that can reach and outgrow in the
181 lungs. In addition to the reduction in barcode number following immunotherapy
182 treatment, we also saw a significant reduction in barcode diversity as measured
183 using the Shannon diversity index (Fig 3F). This indicates that immunotherapy is
184 leading to the immunoediting of specific clonal cell populations over others.

185 To further understand the key immune cell types that control clonal outgrowth in
186 the metastatic lungs we depleted either CD8 T cells (anti-CD8) or NK cells (anti-
187 asialo-GM1) in wildtype mice starting one day prior to tumour resection. Neither
188 treatment led to a significant change in overall survival (Sup Fig 2A). However,
189 depletion of either cell type led to an increase in the number of clones detected
190 within the lungs, reaching statistical significance with T-cell depletion (Fig 3G).

191 This indicates that CD8 T cells and perhaps NK cells play a role in eliminating
192 metastatic clones within the lungs.

193 These results were reproducible, as demonstrated by a second pool of barcoded
194 4T1 cells containing a larger barcode library (300 000 barcodes). Following the
195 injection of 50 000 barcoded cells we recovered approximately 10 000 - 12 000
196 barcode sequences from each primary tumour and this was relatively unchanged
197 in the NSG mice (Sup Fig 3A). This suggests that roughly a fifth of the injected cells
198 are able to engraft and grow in the mammary gland. As clone diversity was
199 unchanged in NSG mice this confirms that the immune system does not play a
200 major role in restricting growth of 4T1 carcinoma cells in the primary tumour
201 setting. In contrast when we examined the number of clones that had spread to
202 the lungs of NSG mice we again found approximately 3 times as many when
203 compared to the wild-type mice (Sup Fig 3A). In addition, we similarly saw a ~3-
204 fold reduction in barcode diversity in response to immunotherapy (Sup Fig 3B).
205 Due to the high complexity of the 300 000 barcode library each mouse received
206 only a partially overlapping complement of barcode clones.

207 **Patterns of enrichment and depletion of specific clones**

208 To better understand how specific clonal cell populations responded to the
209 immune system and immunotherapy we combined the barcode frequencies from
210 the two datasets utilising the 5000 barcode library (WT vs NSG and Control vs
211 Immunotherapy). We performed unsupervised hierarchical clustering of these
212 samples and selected barcodes that were observed at greater than 5% frequency
213 in any one sample. We found that the primary tumours from the two experiments
214 cluster together irrespective of the immune status of the mouse (Balb/c or NSG),
215 further suggesting that 4T1 cells do not undergo immunoediting at the primary
216 site (Fig 4A). In contrast, lung tumours formed in the NSG hosts did not cluster
217 with lung tumours formed in Balb/c lungs, with the immunotherapy treated
218 samples mostly clustering alone or with metastases formed in WT mice. A number
219 of specific barcodes were enriched in the metastatic lungs of all the NSG mice
220 indicating these clones were highly metastatic (Fig 4A). This agrees with the
221 findings of Wagenblast and colleagues (*23*).

222 We identified a number of barcodes that had striking patterns of enrichment or
223 depletion in response to the immune system and immunotherapy, we replotted
224 these using a dot plot (Fig 4B). As these barcodes were enriched or depleted in a
225 reproducible manner across replicate mice this suggests these are due to inherent
226 features of these clones. Firstly, there are three barcodes that were enriched
227 within the NSG lungs (NSG1-3), observed at lower abundance in the untreated
228 wild-type mice, and that were completely eliminated following immunotherapy
229 treatment. This suggest that while these clones are highly metastatic in the
230 absence of an immune system, they are immunogenic and are thus subjected to
231 immunoediting in WT mice particularly following immunotherapy. Another group
232 of metastatic clones that were present in the lungs from NSG and WT mice were
233 further enriched following immunotherapy (IE1-2). These immunotherapy
234 enriched clones were detected in the lungs of all six replicate mice. With the
235 dramatic reduction in the number of barcodes present following immunotherapy,
236 the odds ratio of this happening by chance is 0.0034 (95% confidence interval:
237 0.0010-0.0079; chi square p value: 3.67×10^{-251}). This suggests that these clones

238 have a pre-existing resistance phenotype and are positively selected for following
239 immunotherapy.

240 To further analyse how specific barcodes were enriched in lung metastases
241 following immunotherapy we visualised the top nine clonal populations (based on
242 average barcode proportions in the metastatic lungs) and generated fish-plots.
243 These showed that different clones were preferentially enriched in the lungs of
244 NSG mice when compared to WT mice (Fig 4C). Furthermore, we observed that a
245 small subset of clones were highly enriched in the lungs of immunotherapy treated
246 mice (Fig 4D).

247 **Analysis of immunotherapy resistant clones**

248 To understand more about the phenotype of these immunotherapy resistant
249 clones we established clonal cell populations from two of them (designated IE1
250 and IE2), and two independent control clones (NT1 and NT2) that were not
251 enriched following immunotherapy (3-4 independent clonal cell lines were
252 generated per barcode). These clonal cell lines were isolated from the parental
253 barcoded 4T1 cell population purely *in vitro* with no additional selective
254 manipulation. The barcode within each of these clonal cell lines was confirmed to
255 be correct using Sanger sequencing. All four clonal cell lines had similar growth
256 kinetics *in vitro* indicating no proliferative advantage of the immune evasive
257 clones *in vitro* (Sup Fig 4A).

258 **Genomic analysis for barcode integration site and copy number variation**
259 **(CNV)**

260 To identify the barcode integration sites and determine whether the clones
261 contained large scale genomic alterations we performed whole genome
262 sequencing (WGS) at around 30x coverage of the clones. The WGS analysis
263 determined the precise genomic location at which the barcodes integrated (Sup
264 Table 1). IE1 integrated in the intergenic region between Kpna2 and Smurf2 and
265 IE2 within an intron of Nrf1, neither integration site changed the coding sequence
266 of these genes. Copy number analysis determined that no clone demonstrated
267 dramatic copy number changes when compared to the other clones. Each clone
268 only contained a small number of single copy number gains and losses (IE1 only 6
269 CNVs and IE2 only 5 CNVs), with clone NT2 showing the greatest number of CNVs
270 at 41 (summarised in Sup Table 2). We found one locus with a single copy number
271 gain in both IE1 and IE2 that led to 3 copies of the genes *Nc3r1* (the Glucocorticoid
272 receptor) and *Arhgap26* a Rho GTPase that associates with focal adhesion kinase
273 (FAK), however, this gain was also present in the NT2 clone. These results
274 demonstrate that large scale genomic changes likely do not play a large role in the
275 various phenotypes of the different clones but suggest that copy number changes
276 may be selected against during immunoediting.

277 **Transcriptomic analysis of the clonal cell lines**

278 To investigate the mechanism of immune evasion by these clones we performed
279 RNAseq analysis and compared the two immunotherapy resistant clones to the
280 bulk 4T1 population. The IE1 clone had 1553 differentially expressed genes (Log
281 fold change >2 and FDR $p<0.05$) with 478 significantly upregulated and 1075
282 significantly downregulated (Fig 5A). The IE2 clone had 1099 differentially
283 expressed genes with 375 significantly upregulated and 724 significantly

284 downregulated (Fig 5B). The non-target clones had fewer gene expression
285 changes compared to the bulk 4T1 population with NT1 having 621 and NT2
286 having only 262 differentially expressed genes. We examined the top differentially
287 expressed genes between each of IE1 and IE2 with the parental 4T1 cells,
288 however, we did not find any with an obvious role in immune evasion (Sup Tables
289 3 & 4). Gene set enrichment analysis revealed that two of the top ten gene sets
290 were upregulated in both IE1 and IE2 (CHEN_HOXA5_TARGETS_9HR_UP,
291 BLUM_RESPONSE_TO_SALIRASIB_UP), while most were unique to either cell line
292 (Sup Tables 5 & 6). *Hoxa5* is a known tumour suppressor gene in breast cancer
293 (*27*) and although we see an enrichment of its target genes, the expression of
294 *Hoxa5* itself was significantly reduced in the IE1 clone and there was a trend to
295 reduced expression in the IE2 clone. There was no overlap in the top ten down
296 regulated gene-sets between IE1 and IE2. The top downregulated gene-set for IE1
297 was the REACTOME_UB_SPECIFIC_PROCESSING_PROTEASES gene-set, that
298 contained two genes involved in antigen processing for display by MHC-I (*Psmb8*
299 and *Psmb9*). As down regulation of the MHC-I pathway is a common mechanism
300 of immune evasion we investigated this in more detail.

301 Through this analysis we found that the IE1 clone had significantly reduced
302 expression of many genes related to antigen presentation including MHC-I (*H2-*
303 *k1*), *Tap2*, *Psmb8*, *Psmb9* and *Psmb10* (Fig 5C). *H2-k1* is the main MHC molecule
304 expressed by the Balb/c strain of mouse that the 4T1 carcinoma cell line was
305 derived from. We validated the reduction in MHC-I expression levels seen in the
306 RNAseq data at the protein level using flow cytometry (Fig 5D). This analysis
307 showed that the IE1 clone had significantly reduced cell surface MHC-I protein
308 expression compared to the bulk 4T1 population. We thus examined the WGS data
309 and this showed that the loss of MHC-I expression in IE1 was not due to genomic
310 loss at the MHC locus on chromosome 17 (Sup Fig 5A. In contrast the IE2 clone
311 had elevated levels of a number of these MHC related genes (Fig 5C), in addition
312 to a non-classical MHC molecule *H2-t23* (Fig 5E) that is known to negatively
313 regulate NK cells through their inhibitory receptor *Nkg2a* (*28*). Interestingly IE2
314 cells also demonstrated a significantly increased expression of the T cell inhibitory
315 molecule *Cd274*/PD-L1 (Fig 5E). This again was validated at the protein level using
316 flow cytometry (Fig 5F). These results demonstrate that each of the two
317 immunotherapy resistant clones are phenotypically unique.

318 We next examined whether the copy number changes or barcode integration sites
319 identified above impacted gene expression. In IE1 and IE2 the copy number
320 changes in *Nc3r1* (the Glucocorticoid receptor) and *Arhgap26* were associated
321 with significantly increased expression of these genes but NT2 demonstrated no
322 change in expression (Sup Fig 5B). Elevated Nc3r1 expression has been associated
323 with poor prognosis and metastasis in TNBC although whether it plays a role in
324 immune evasion is not known (*29, 30*). As stated above the barcode for IE1
325 integrated in the intergenic region between Kpna2 and Smurf2 and IE2 within an
326 intron of Nrf1. The expression of Smurf2 was the only of these genes that was
327 significantly altered with a modest log fold increase of 0.59 in IE1.

328 **Demethylating drugs do not fully restore MHC expression**

329 Demethylating agents such as 5-aza-2'-deoxycytidine (5-aza) are known to
330 upregulate MHC-I expression in cancer cells (*31*), thus we treated our clonal cell

331 lines utilising 5-aza for 72 hours to determine whether DNA methylation was a
332 mechanisms suppressing MHC expression in the IE1 clone. Using flow cytometry,
333 we observed that MHC-I expression was elevated in a dose dependent manner
334 following 5-aza treatment in all clones. However, MHC-I expression in the IE1
335 clone was consistently lower than the parental 4T1 cell line at all doses of 5-aza
336 (Sup Fig 6A). This indicates that gene hyper-methylation is not the mechanism of
337 MHC-I suppression in the IE1 clone.

338 IFN-gamma stimulation is another mechanism by which MHC expression can be
339 increased on cancer cells. The IE1 clone responded to IFN-gamma treatment by
340 upregulating MHC-I expression but again it remained suppressed compared to the
341 parental 4T1 cells (Sup Fig 6B). This suggests these cells broadly retain the
342 transcriptional regulatory machinery that is required to upregulate MHC-I in
343 response to IFN-gamma stimulation. These results indicate that MHC
344 downregulation is likely regulated by epigenetic factors other than DNA
345 methylation and that the majority of MHC expression in this clone can be restored
346 by IFN-gamma treatment.

347 **Overlapping gene signature predicts poor survival in breast cancer patients**

348 We had noted that the GSEA analysis showed some overlap in enriched gene-sets
349 between the two immune evasive clones (IE1 and IE2), we thus reasoned that as
350 well as having unique immune evasion features these clones may have some
351 pathways in common. To identify the common immune evasion pathways being
352 initiated by both the immunotherapy resistant clones we generated Venn
353 diagrams to identify overlapping gene expression changes (Sup Table 7). This
354 analysis demonstrated that the immunotherapy resistant clones had more gene
355 expression changes in common with each other and less in common with the
356 control non-target clones (Fig 6A). We generated a heatmap of the top 50
357 upregulated and downregulated genes across all the samples (Fig 6B) and
358 performed GSEA analysis using C2 on the longer list (Sup Fig 7A, Sup Table 8).
359 Only two gene sets had significant p values when you consider multiple testing,
360 these were the HOXA5 gene set mentioned previously and a COVID19 related gene
361 set. Although not significant there were several additional COVID19 related gene
362 sets from the same recent publication identified in the overlapping upregulated
363 gene list suggesting an immune related role of these genes (*32*).

364 Therefore we wanted to understand the role of these genes in patients, so we
365 generated signatures from the top 25 upregulated and downregulated genes that
366 had human orthologs and were detectable in both the METABRIC (*33*) and TCGA
367 datasets (*34*). We then analysed the role of these signatures in survival using the
368 basal-like breast cancer patients from these cohorts. While the patients in these
369 cohorts have not been treated with immunotherapy it has previously been
370 demonstrated that immune features such as the number of tumour infiltrating
371 lymphocytes or regulatory T cells influence prognosis in basal-like breast cancer
372 patients (*35*). When we analysed overall survival in these cohorts we observed
373 that the upregulated signature associated with substantially poorer outcome in
374 both cohorts (METABRIC: p=0.0043, HR=2.0, Fig 6C; TCGA: p=0.042, HR=4.3, Fig
375 6D). In contrast the downregulated gene signature did not show any significance
376 in either cohort (data not shown). We generated heatmaps with unsupervised
377 clustering to determine whether specific genes or groups of genes from the

signature were specifically driving the association with survival (Sup Fig 7B). In the TCGA data we observed a number of clusters that seemed to associate more with survival, one of these included the genes *FAM71F2, MASP2, HLF, PPP1R15A, MMP23B* and *LIMS2*. Interestingly one of these genes *Ppp1r15a* also known as GADD34 has previously been demonstrated to be critical in blocking immunogenic cell death following chemotherapy, and when it was inhibited the chemotherapy response was improved in immunocompetent mice but not immunocompromised mice (*36*). A second group of genes included *SEZ6L2* and this gene has been associated with survival in a number of cancers but not through an immune related mechanism (*37, 38*). There was no enrichment of proliferation or invasion gene sets in our GSEA analysis suggesting that these processes were not behind the poor outcome of patients that highly express genes in the common upregulated signature.

Previous studies have shown that CTL infiltration correlates with survival in basal-like breast cancer so it is possible our signature is a surrogate measure of T cell infiltration. To test this, we performed TIDE analysis (*39*) on the TCGA and METABRIC cohorts followed by correlation analysis between the CTL signature score and our upregulated immune evasion signature score. This showed no correlation in the METABRIC cohort and only a weak negative correlation in the TCGA cohort (Sup Fig 7C) suggesting little overlap between these two predictors of patient survival. Future studies will be necessary to determine how the genes in this signature regulate survival, influence immune evasion and immunotherapy response.

Discussion:

Immunotherapy is revolutionising cancer therapy, with dramatic long-term responses seen in certain patient groups. Unfortunately, other patients see limited response to the current immunotherapies, and in particular some cancer types such as breast cancer are less responsive in general. Thus, our understanding of immune evasion in non-responsive cancer types needs significant improvement. We looked to address this by examining the fundamental pattern of immune evasion at a clonal level, and furthermore to use this information to identify pathways that could be targeted to overcome immunotherapy resistance. Using cellular DNA barcoding, we have demonstrated that the immune system shapes clonal evolution of primary and metastatic cancer cells in syngeneic models of basal-like breast cancer. Additionally, we have demonstrated that a second round of immunoediting occurs during metastasis and thus immune evasion at the primary site does not guarantee immune evasion during metastasis. DNA barcoding allows for tracking of specific clones with exquisite sensitivity. We find that immunotherapy enhances immunoediting at both the primary tumour and metastatic sites. Finally, we identify a common immune evasion gene signature in metastatic clones that is predictive of survival in basal-like breast cancer patients.

Here we show, for the first time in a solid tumour, that clonal immunoediting occurs in response to immunotherapy. Using the more immunotherapy sensitive EMT6 model we demonstrate that immunoediting occurs at the primary tumour site and that immunotherapy leads to strong clonal selection. The more immunotherapy resistant 4T1 model demonstrated that while most 4T1 cells are able to evade the immune system at the primary site, only a subset of these cells

426 are able to evade the immune system during metastasis. This indicates immune
427 evasion is not a static process but requires ongoing regulation through tumour
428 progression, even in a highly aggressive allograft model. These findings agree
429 broadly agree with recent comprehensive genomic analysis of patient samples
430 assessed across metastatic sites and over time (*3, 40*). These studies tracked clonal
431 populations in metastatic lesions using whole genome sequencing, examined a
432 number of immune correlates and could identify immunoediting that was
433 associated with the immune response. However, they were unable to examine
434 clonal heterogeneity driven by epigenetic or transcriptomic changes and were
435 limited in identification of rare clones by sequencing depth. Future clinical studies
436 utilising single cell approaches to analyse multiple biopsies from individual
437 patients over a time-course of treatment will be necessary to confirm the key
438 findings of this study in patients. While extremely challenging these studies are
439 becoming more feasible with recent technological improvements.

440 Our study and that of others have indicated that immunoediting can be mediated
441 by both CD8 T cells and NK cells (*13, 14*). In addition, immunoediting can select for
442 clones with more immune evasive phenotypes irrespective of specific neoantigens
443 (*2, 4, 6*). The only previous study examining immunoediting at a clonal level, used
444 a fluorescent barcoding approach in a B cell leukemia model (*12*). While our
445 findings broadly agree with the findings of this study, the study by Milo and
446 colleagues was limited to five unique fluorescent clones that could be tracked, and
447 were confounded by the variable immunogenicity of each of the different
448 fluorescent proteins. Our DNA barcoding approach in contrast allowed for the
449 labelling of thousands of clones and a much more precise identification of immune
450 evasive clones. We could then isolate these specific clones and identify both
451 common and variable features of immune evasion in individual clones.
452 Furthermore, this technique unlike a fluorescent barcode approach allowed us to
453 determine that pre-existing clones existed in both the EMT6 and 4T1 models that
454 had greater immunotherapy resistance, as these exact clones were enriched from
455 the same starting pool of cells across replicate mice.

456 We identified and isolated two of the immunotherapy resistant clones from the
457 4T1 model, based on their unique barcodes. In depth analysis of these resistant
458 clones demonstrated they had differential gene expression of key immune evasive
459 pathways (MHC-I and PD-L1). Intratumoural heterogeneity (ITH) has previously
460 been associated with immune evasion and resistance to immunotherapy in
461 melanoma and lung cancer. Tumours with higher ITH were shown to be more
462 resistant to immunotherapy (*41, 42*). McGranaham and colleagues postulated that
463 this was due to improved T cell killing of tumours with clonal neo-antigens.
464 Another non-mutually exclusive explanation is that clonal tumours are less likely
465 to contain cancer cells with a pre-existing resistance mechanism to
466 immunotherapy. These findings refine the concept of cancer immunoediting,
467 demonstrating that there are clonal populations of cancer cells with variable
468 resistance to the immune system. Based on their phenotype these clones are
469 either enriched or depleted by an active immune system and immunotherapy.

470 We identified a core overlapping gene expression profile between the
471 immunotherapy resistant clones. The common upregulated gene signature
472 showed a dramatic ability to stratify basal-like breast cancer patients into good
473 and poor prognosis. This gene signature appeared to represent a novel immune

474 evasion pathway associated with poor prognosis. Aside from *Ppp1r15a* it did not
475 have genes known to be associated with immune evasion, and in addition did not
476 contain genes associated with other poor prognostic signatures such as
477 proliferation or invasion.

478 Importantly as both T cells and NK cells are present during immunoediting in our
479 model system this common signature likely enables the cancer cell clones to evade
480 both T cells and NK cells. Interestingly our common signature did not strongly
481 correlate with CTL infiltration as determined by TIDE analysis (*39*), indicating that
482 this signature was not a surrogate for the lack of T cell infiltration. This also
483 suggests these genes likely do not regulate immune evasion by influencing
484 immune cell recruitment. These common genes may offer new insights into
485 developing therapeutic approaches to improve immunotherapy response in
486 breast cancer. One of the common immunotherapy resistance genes we identified
487 was *PPP1R15A* that may be important in immunotherapy response. Our
488 identification of *PPP1R15A* as elevated in immuno-resistant clones is consistent
489 with its known role in immunogenic cell death in the response to chemotherapy
490 (*36*). Some recent studies in another disease setting have demonstrated that this
491 pathway can be targeted using a small molecule (Sephin-1), where it was used to
492 treat a mouse model of multiple sclerosis (*45*). Future studies are necessary to
493 examine whether this compound or others targeting this pathway could synergise
494 with immunotherapy, or immunogenic chemotherapy to treat breast or other
495 cancer types.

496 As breast cancers have a lower mutational burden than lung cancer and melanoma
497 it is likely that epigenetic factors may play a greater role than mutational events
498 in driving ITH in breast cancer. One current approach to improve immunotherapy
499 response under investigation has been to combine immunotherapy with
500 epigenetic targeting drugs such as decitabine and HDAC inhibitors (*31, 43*). This
501 combination has been shown to lead to an upregulation of MHC protein expression
502 and improved response to immunotherapy. However, the use of epigenetic drugs
503 might have an additional effect of reducing ITH in certain immune evasion
504 pathways. Thus, epigenetic drugs may reduce the diversity of clones and
505 overcome other epigenetically driven immune evasion strategies as well as
506 enhancing MHC expression (*44*). Further research is needed to test this hypothesis
507 more fully. Our results, however, suggest that while demethylating agents could
508 increase MHC-I expression in the MHC-I low immunotherapy resistant clone, they
509 did not increase it above the baseline seen in the parental 4T1 cell line. This is
510 corroborated by a recent study that demonstrated that while treating breast
511 cancer patients with demethylating agents could increase MHC-I expression in
512 most patients, a subset appeared resistant to this therapy (*31*). This suggests that
513 while epigenetic treatments may improve the proportion of patients who respond
514 to immunotherapy that in some cases pre-existing clones could still mediate
515 resistance to this combination.

516 Some limitations of this study include the reliance on mouse cell line models, as
517 these do not recapitulate the early stages of tumorigenesis and do not represent
518 the full diversity of human breast cancer. However, syngeneic allograft models
519 have delivered central insights about the immune response to cancer and
520 demonstrated the utility of immunotherapies (*46*). A further limitation is that the
521 integration of the barcode and selection markers into the genome and the

522 potential immunogenicity of the RFP could affect the phenotype of the cancer cells.
523 In previous studies we and others have found some fluorophores and luciferase to
524 be immunogenic and negatively affect tumour growth and metastasis in the 4T1
525 model (*24, 47*). However, in this study we found that tumour growth and
526 metastasis were unaffected by RFP expression. While the introduction of the DNA
527 barcodes could have influenced the phenotype of the specific clones we feel that
528 this is unlikely, with no dramatic impact on the expression of the genes closest to
529 the integration site. Furthermore, none of the genes associated with each
530 integration site came out as being significantly involved in cancer cell evasion of
531 CD8 T cell responses in a recent CRISPR screen (*15*).

532 Overall this study has demonstrated that immunoediting occurs at the clonal level
533 in primary tumours and that a second round of immunoediting occurs during
534 metastasis. Immunotherapies dramatically enhanced immunoediting, however,
535 pre-existing resistant populations were still responsible for relapse. The large
536 reduction in clonal diversity following immunotherapy in the 4T1 model, a model
537 that is known to be poorly responsive to immunotherapy, suggests that slight
538 improvements through combination therapy could eliminate the remaining clones
539 and lead to dramatic improvements in survival. By isolating immunotherapy
540 resistant clones and phenotyping them, we identified common and distinct
541 immune evasion pathways. We anticipate through the targeting of the pathways
542 identified in this study, in particular the common pathways, it will be possible to
543 further reduce the numbers of resistant clones and improve the efficacy of
544 immunotherapies.
545
546 **Acknowledgments**
547
548 This work is supported by a research grants from The National Breast Cancer
549 Foundation (NBCF) of Australia (IN-17-02; IIRS-19-106) and supported by the
550 generosity of John McMurtrie (AM) and Deborah McMurtrie and The Petre
551 Foundation. LAB is the recipient of an Australian Government research training
552 (RTP) scholarship. AS is the recipient of a Senior Research Fellowship from the
553 National Health and Medical Research Council of Australia. SJ is supported by a
554 research fellowship from the NBCF. We acknowledge the contribution of Isabelle
555 Shapiro and Cheryl Grant as consumer advocates.
556
557
558 **Methods:**
559 Cells
560 4T1 cells were obtained from ATCC. 4T1 cells were grown in RPMI (Gibco)
561 supplemented with 10% FCS, D-Glucose, Sodium Pyruvate, 2mM HEPES, and
562 Penicillin/Streptomycin. EMT6 cells were obtained from ATCC. EMT6 cells were
563 grown in Waymouth's MB 752/1 Medium supplemented with 15% FCS and 2mM
564 L-glutamine.
565
566 Cellular DNA barcoding
567 The ClonTracer library was a gift from Dr Frank Stegmeier (Addgene #67267).
568 Lentiviral particles containing the high-complexity barcode library were
569 produced by transfecting 293T cells. 4T1 and EMT6 cancer cell lines were
570 barcoded by lentiviral infection using 0.8 μg/ml polybrene. Cells from each line,

571 were infected with a target MOI of 0.1, corresponding to 10% infectivity to ensure
572 single lentiviral integration. Cells that received a barcode were then sorted based
573 on the RFP reporter protein using a BD FACSAriaII, these cells were then expanded
574 and frozen into a number of aliquots for the subsequent experiments. 4T1 cells
575 were generated with two different barcode complexities, one with ~5000
576 barcodes (4T1 BC5000) and one with ~300 000 barcodes.
577
578 Mice
579 All animal experiments were approved by the Garvan Institute of Medical
580 Research/St. Vincent's Hospital Animal Experimentation Ethics Committee.
581 Immunocompetent BALB/c mice and immunocompromised NOD.Cg-*Prkdc*^{scid}
582 *Il2rg*^{tm1Wjl}/SzJ (NSG) mice aged 6-to-8 weeks were obtained from Australian
583 BioResources (Moss Vale, Australia) and housed at the Garvan Institute of Medical
584 Research.
585
586 *In vivo* tumour growth
587 For tumour transplantation, barcoded EMT6 cells (ATCC, USA) were resuspended
588 in Matrigel 2.5x10^5 cells in 100ul volume were injected into the 4th inguinal
589 mammary gland; barcoded 4T1 cells (ATCC, USA) were resuspended in PBS and
590 5x10^4 cells in a 10ul volume were injected into the 4th inguinal mammary fat pad.
591 For studies with the 4T1 model primary tumours were surgically resected at day
592 15. At resection or ethical endpoint tumours and metastatic lung tissue were
593 removed, minced and snap frozen in liquid nitrogen for barcode analysis.
594
595 Immunotherapy treatment
596 Mice were treated with four 200ug doses of either combination immunotherapy
597 antibodies via intraperitoneal injection: anti-CTLA4 (BE0032), anti-PD1
598 (BE0146), or isotype control antibodies Armenian hamster IgG (BE0091), Rat IgG
599 (BE0089) all from BioXCell (Lebanon, NH, USA). Antibodies were given every 2-3
600 days from day 10 post tumour implantation for the EMT6 model and following
601 resection on day 15 for the 4T1 model.
602
603 CD8 T cell and NK cell depletion
604 Starting one day prior to primary tumour resection mice were given 100ug of
605 depleting antibodies for CD8 T cells (anti-CD8; BEO223; BioXCell), or NK cells
606 (anti-Asialo-GM1; 986-10001; Novachem), or isotype control antibodies.
607 Antibodies were then given every 2-3 days for a total of 4 doses.
608
609 DNA extraction
610 Frozen tissue samples were lysed in 5 ml QIAGEN buffer P1 (with RNaseA) and
611 0.5% SDS within a Miltenyi M-Tube (# 130-096-335). Samples were processed
612 on the gentleMACS or gentleMACS Octo using the RNA_02 program. DNA was
613 then extracted using a standard phenol/chloroform process.
614
615 Targeted Barcode PCR and Sequencing
616 All samples underwent targeted barcode PCR amplification according to the
617 updated version of the original protocol (*22*) available on the Addgene website
618 (https://www.addgene.org/pooled-library/clontracer/). Specific PCR products
619 (180 bp) were gel purified, quantified by Qubit 2.0 fluorometer (ThermoFisher

620 Scientific, Waltham, MA USA) and pooled into a library. Prior to sequencing, an
621 equal combination of additional PCR products containing two inverse barcodes
622 (GACTCAGTGTCAGACTGAGTGTCTGACTGT and
623 CTGAGTCACAGTCTGACTCACAGACTGACA) plus the PhiX Control V3 (Cat. FC-110-
624 3001, Illumina, CA, USA) were spiked in to balance the nucleotide distribution
625 within the library. Samples were sequenced using a custom sequencing primer
626 (GCGACCACCGAGATCTACACACTGACTGCAGTCTGAGTCTGACAG) and the
627 NextSeq® 500/550 Mid Output Kit v2 - 150 cycles (FC-404-2002, Illumina, CA,
628 USA) on the Illumina NextSeq® platform.
629
630 Barcode Analysis
631 Barcode composition analysis and calculation of barcode overlap between
632 samples was performed as indicated in the original protocol (*22*) and updated
633 Python scripts available from the Addgene website
634 (https://www.addgene.org/pooled-library/clontracer/).
635 Further analysis was performed using R statistical framework and packages
636 EntropyExplorer for analysis of differential Shannon Entropy (*48*), DEBRA for
637 differential barcode expression (*49*), and libraries fishplot and UpSetR for
638 visualisation purposes.
639
640 Generating clonal cell lines
641 Cells of interest were isolated from the barcoded parental population using a sub-
642 pooling approach.
643 The barcoded 4T1 BC5000 cells were seeded into a 96 well plate at a density of
644 150 cells per well. At approximately 80% confluence, cells were trypsinised and
645 split identically into two plates. One plate was viably frozen in freezing media
646 (10% DMSO, 40% FCS, 50% 4T1 media). DNA was extracted from one plate using
647 the Promega SV Wizard Genomic DNA kit. Target barcodes of each sample were
648 PCR amplified and sequenced using the method described above.
649 After sequencing, wells containing cells with the target barcodes were thawed,
650 pooled and seeded at 40 cells/well in a 96 well plate. Media was changed every
651 three days for 8 days before cells were split into two identical plates as above. One
652 plate was viably frozen in freezing media, while DNA was extracted and prepared
653 for targeted sequencing as above.
654 Wells with the highest proportion of target barcodes were revived into a 6 well
655 plate and grown for 4 days before being single-cell sorted by BD FACSAria II into
656 96 well plate. Sorted single cells were grown in conditioned media for 5 days
657 before being changed to 4T1 media and grown until 80% confluence. As
658 previously, cells were lifted and split identically into two plates – one for freezing
659 and one for targeted sequencing.
660 Once wells containing single cells clones of the cells of interest were identified,
661 target wells were revived. Cells were expanded before being aliquoted and viably
662 frozen for future experiments.
663 Barcoded sequences of isolated cells were confirmed by targeted Sanger
664 sequencing of barcode regions.
665
666 Bulk RNA sequencing
667 RNA was extracted from established subclonal cell lines using the QIAGEN RNeasy
668 Mini Kit. 3-4 unique clonal cell populations were sequenced for each barcode.

669 Libraries were prepared using the KAPA RNA HyperPrep Kit with RiboErase, and
670 sequenced on the NextSeq500 platform using a High Output V2.5 300 cycle kit.
671
672 Transcriptome analysis
673 FastQ files from sequencing libraries were first trimmed with FASTQC v0.11
674 *Andrews S. (2010). FastQC: a quality control tool for high throughput sequence data.*
675 *Available online at: http://www.bioinformatics.babraham.ac.uk/projects/fastqc*.
676 Raw reads were subsequently mapped to the mouse transcriptome (Gencode
677 release M9, GRCm38.p4), to the mouse genome (mm10 assembly), with STAR
678 aligner v.2.4.1d, allowing for multimapping reads (*50*). The reads were counted
679 over gene models with RSEM, v.1.2.18 (*51*). Differentially expressed genes and
680 repeat elements were defined with EdgeR with FDR<0.01 (*52*).
681
682 Survival analysis
683 To assess the clinical relevance of our isolated immune evasion clones, we
684 assessed the association between the gene signatures derived from our bulk RNA-
685 Sequencing studies with the overall survival of basal (PAM50) breast cancer
686 patients from the METABRIC and The Cancer Genome Atlas (TCGA;
687 https://www.cancer.gov/tcga) cohorts. Mouse gene signatures were first
688 converted to human orthologs using the biomaRt package (*53*). Shared up-
689 regulated genes across both immune evasion clones IE1 and IE2 were then
690 filtered, and only genes detected in each expression cohort were considered. For
691 each tumour from the bulk cohort, signature scores were computed based on the
692 average expression of the top 25 genes ranked by log fold change. Patients were
693 then stratified based on the signatures scores into the top 30%, middle 40% and
694 bottom 30% groups. Survival curves were generated using the Kaplan Meier
695 method with the 'survival' package in R (https://cran.r-
696 project.org/package=survival). The Cox proportional hazards model was used to
697 compute Hazard Ratios. We assessed the significance between groups using the
698 log-rank test statistics.
699
700 Whole genome sequencing
701 DNA was extracted from established subclonal cell lines using the QIAGEN DNeasy
702 blood & tissue kit. Libraries were prepared using the Roche KAPA PCR-free library
703 preparation kit and genomes were sequenced on the HiSeq X platform to a depth
704 of ~30x.
705
706 Whole genome analysis
707 Fastq files from the WGS were firstly aligned to mouse genome reference mm10.
708 The output bam files were subsequently used for copy number analysis. Copy
709 number analysis was performed using a R package cn.mops (*54*) in "paired mode"
710 with a window length of 10kb. Reads were aligned to the BALB/c reference
711 genome using BWA before being indexed and sorted with Novosort. Reads that
712 mapped incompletely to the reference genome were then mapped to the barcode
713 plasmid sequence with BWA and sorted and indexed with Novosort. Read pairs
714 where only one pair mapped to the barcode plasmid sequence were blasted
715 against mm10 to establish the barcode plasmid insertion site.
716
717

718 Flow cytometry for MHC1 and PD-L1
719 The 4T1 subclones (IE1, IE2, NT1, NT2), as well as the parental 4T1 bulk
720 population were revived and passaged three times before being seeded into a 6
721 well plate at a density of 200 000 cells per well. At approximately 80% confluence,
722 cells were collected into FACS buffer (DPBS supplemented with 2% FCS and 2%
723 HEPEs) for flow cytometry. Cells were stained with a mastermix of APC conjugated
724 anti-mouse CD274 (Biolegend) and Alexa Fluor488 conjugated anti-mouse H2-kD
725 (Biolegend) at a final concentration of 1:200 for 20 minutes. Cells were washed
726 three times with FACs buffer before being stained with DAPI and run on the BD
727 FACSCanto II flow cytometer, utilising BD FACSDIVA software. Data was analysed
728 in FlowJo (version 10.6.1) and median fluorescence intensity of live, single cells
729 was calculated.
730
731 Treating cells with 5-Aza-2'-deoxycytidine and flow cytometry for MHC-I
732 5-Aza-2'-deoxycytidine (5aza) was sourced from Sigma and reconstituted in
733 DMSO according to manufacturer's instructions. Subclones (IE1, IE2) and the
734 parental 4T1 cell line were seeded into a 24 well plate at a density of 8000 cells
735 per well in 4T1 media (previously described). Cells were allowed to settle
736 overnight before being treated with 5aza at 200nM, 100nM or 50nM for 72 hours.
737 5aza was removed and cells were cultured in media only for 24 hours before being
738 collected for flow analysis. Cells were stained with Alexa Fluor488 conjugated
739 anti-mouse H2-kD (Biolegend) at a concentration of 1:200 in FACS buffer for 20
740 minutes. Cells were washed three times after staining before being stained with
741 DAPI. Data was collected using the BC FACSCanto II flow cytometer with BD
742 FACSDIVA software. The resulting data was analysed using FlowJo (version
743 10.6.1) and media fluorescence intensity of live, single cells was calculated.
744
745 Treating cells with interferon gamma and flow cytometry for MHC-I
746 Active mouse interferon gamma (IFNγ) was sourced from Abcam and
747 reconstituted in sterile water, as per manufacturer's instructions. Subclones (IE1,
748 IE2) and the parental 4T1 cell line were grown in a 24 well plate until
749 approximately 70% confluence was achieved. Cells were then treated with IFNγ
750 (100ng/ml) for 24 hours. Cells were stained with Alexa Fluor488 conjugated anti-
751 mouse H2-kD (Biolegend) at a concentration of 1:200 in FACS buffer for 20
752 minutes. Cells were washed three times before being stained with DAPI. Data was
753 generated using the BC FCSCanto II flow cytometer with BD FACSDIVA software.
754 Analysis was carried out using FlowJo (version 10.6.1) and median fluorescence
755 intensity of live single cells was calculated.
756
757 **References:**
758
759 1. D. Hanahan, Robert A. Weinberg, Hallmarks of Cancer: The Next
760 Generation. *Cell* **144**, 646-674 (2011).
761 2. R. D. Schreiber, L. J. Old, M. J. Smyth, Cancer Immunoediting: Integrating
762 Immunity's Roles in Cancer Suppression and Promotion. *Science* **331**,
763 1565-1570 (2011).
764 3. M. Angelova *et al.*, Evolution of Metastases in Space and Time under
765 Immune Selection. *Cell* **175**, 751-765.e716 (2018).

766 4. S. C. Casey *et al.*, MYC regulates the antitumor immune response through
767 CD47 and PD-L1. *Science* **352**, 227-231 (2016).
768 5. D. M. Pardoll, The blockade of immune checkpoints in cancer
769 immunotherapy. *Nature Reviews Cancer* **12**, 252-264 (2012).
770 6. P. Sharma, S. Hu-Lieskovan, J. A. Wargo, A. Ribas, Primary, Adaptive, and
771 Acquired Resistance to Cancer Immunotherapy. *Cell* **168**, 707-723 (2017).
772 7. L. Galluzzi, T. A. Chan, G. Kroemer, J. D. Wolchok, A. López-Soto, The
773 hallmarks of successful anticancer immunotherapy. *Science Translational*
774 *Medicine* **10**, (2018).
775 8. P. Schmid *et al.*, Atezolizumab and Nab-Paclitaxel in Advanced Triple-
776 Negative Breast Cancer. *New England Journal of Medicine* **379**, 2108-2121
777 (2018).
778 9. H. R. Ali, L. Chlon, P. D. P. Pharoah, F. Markowetz, C. Caldas, Patterns of
779 Immune Infiltration in Breast Cancer and Their Clinical Implications: A
780 Gene-Expression-Based Retrospective Study. *PLOS Medicine* **13**, e1002194
781 (2016).
782 10. E. T. E. Gross *et al.*, Immunosurveillance and immunoediting in MMTV-
783 PyMT-induced mammary oncogenesis. *Oncoimmunology* **6**, e1268310
784 (2017).
785 11. C. M. Koebel *et al.*, Adaptive immunity maintains occult cancer in an
786 equilibrium state. *Nature* **450**, 903-907 (2007).
787 12. I. Milo *et al.*, The immune system profoundly restricts intratumor genetic
788 heterogeneity. *Science Immunology* **3**, (2018).
789 13. H. Matsushita *et al.*, Cancer exome analysis reveals a T-cell-dependent
790 mechanism of cancer immunoediting. *Nature* **482**, 400-404 (2012).
791 14. K.-J. Malmberg *et al.*, Natural killer cell-mediated immunosurveillance of
792 human cancer. *Seminars in Immunology* **31**, 20-29 (2017).
793 15. K. A. Lawson *et al.*, Functional genomic landscape of cancer-intrinsic
794 evasion of killing by T cells. *Nature*, (2020).
795 16. R. T. Manguso *et al.*, In vivo CRISPR screening identifies Ptpn2 as a cancer
796 immunotherapy target. *Nature* **547**, 413 (2017).
797 17. C.-Q. Song *et al.*, Genome-Wide CRISPR Screen Identifies Regulators of
798 Mitogen-Activated Protein Kinase as Suppressors of Liver Tumors in Mice.
799 *Gastroenterology* **152**, 1161-1173.e1161 (2017).
800 18. G. Wang *et al.*, CRISPR-GEMM Pooled Mutagenic Screening Identifies
801 KMT2D as a Major Modulator of Immune Checkpoint Blockade. *Cancer*
802 *Discovery* **10**, 1912-1933 (2020).
803 19. S. J. Patel *et al.*, Identification of essential genes for cancer immunotherapy.
804 *Nature* **548**, 537-542 (2017).
805 20. N. Anfossi *et al.*, Human NK Cell Education by Inhibitory Receptors for MHC
806 Class I. *Immunity* **25**, 331-342 (2006).
807 21. E. Mamessier *et al.*, Human breast cancer cells enhance self tolerance by
808 promoting evasion from NK cell antitumor immunity. *The Journal of Clinical*
809 *Investigation* **121**, 3609-3622 (2011).
810 22. H.-e. C. Bhang *et al.*, Studying clonal dynamics in response to cancer therapy
811 using high-complexity barcoding. *Nat Med* **21**, 440-448 (2015).
812 23. E. Wagenblast *et al.*, A model of breast cancer heterogeneity reveals
813 vascular mimicry as a driver of metastasis. *Nature* **520**, 358-362 (2015).

24. A. Gambotto *et al.*, Immunogenicity of enhanced green fluorescent protein (EGFP) in BALB/c mice: identification of an H2-Kd-restricted CTL epitope. *Gene Therapy* **7**, 2036-2040 (2000).
25. Y. Lan *et al.*, Enhanced preclinical antitumor activity of M7824, a bifunctional fusion protein simultaneously targeting PD-L1 and TGF-β. *Science Translational Medicine* **10**, (2018).
26. M. Ouzounova *et al.*, Monocytic and granulocytic myeloid derived suppressor cells differentially regulate spatiotemporal tumour plasticity during metastatic cascade. *Nature Communications* **8**, 14979 (2017).
27. X. Peng, L. Zha, A. Chen, Z. Wang, HOXA5 is a tumor suppressor gene that is decreased in gastric cancer. *Oncol Rep* **40**, 1317-1329 (2018).
28. R. E. Vance, J. R. Kraft, J. D. Altman, P. E. Jensen, D. H. Raulet, Mouse CD94/NKG2A Is a Natural Killer Cell Receptor for the Nonclassical Major Histocompatibility Complex (MHC) Class I Molecule Qa-1b. *Journal of Experimental Medicine* **188**, 1841-1848 (1998).
29. M. M. S. Obradović *et al.*, Glucocorticoids promote breast cancer metastasis. *Nature* **567**, 540-544 (2019).
30. D. Pan, M. Kocherginsky, S. D. Conzen, Activation of the Glucocorticoid Receptor Is Associated with Poor Prognosis in Estrogen Receptor-Negative Breast Cancer. *Cancer Research* **71**, 6360-6370 (2011).
31. N. Luo *et al.*, DNA methyltransferase inhibition upregulates MHC-I to potentiate cytotoxic T lymphocyte responses in breast cancer. *Nature Communications* **9**, 248 (2018).
32. D. Blanco-Melo *et al.*, Imbalanced Host Response to SARS-CoV-2 Drives Development of COVID-19. *Cell* **181**, 1036-1045.e1039 (2020).
33. C. Curtis *et al.*, The genomic and transcriptomic architecture of 2,000 breast tumours reveals novel subgroups. *Nature* **486**, 346-352 (2012).
34. N. The Cancer Genome Atlas, Comprehensive molecular portraits of human breast tumours. *Nature* **490**, 61 (2012).
35. S. Dushyanthen *et al.*, Relevance of tumor-infiltrating lymphocytes in breast cancer. *BMC Medicine* **13**, 202 (2015).
36. M. Obeid *et al.*, Calreticulin exposure dictates the immunogenicity of cancer cell death. *Nature Medicine* **13**, 54-61 (2007).
37. N. Ishikawa *et al.*, Characterization of SEZ6L2 cell-surface protein as a novel prognostic marker for lung cancer. *Cancer Science* **97**, 737-745 (2006).
38. L. Wang *et al.*, Upregulated Seizure-Related 6 Homolog-Like 2 Is a Prognostic Predictor of Hepatocellular Carcinoma. *Disease Markers* **2020**, 7318703 (2020).
39. P. Jiang *et al.*, Signatures of T cell dysfunction and exclusion predict cancer immunotherapy response. *Nature Medicine* **24**, 1550-1558 (2018).
40. A. W. Zhang *et al.*, Interfaces of Malignant and Immunologic Clonal Dynamics in Ovarian Cancer. *Cell*, (2018).
41. N. McGranahan *et al.*, Clonal neoantigens elicit T cell immunoreactivity and sensitivity to immune checkpoint blockade. *Science* **351**, 1463-1469 (2016).
42. Y. Wolf *et al.*, UVB-Induced Tumor Heterogeneity Diminishes Immune Response in Melanoma. *Cell* **179**, 219-235.e221 (2019).

43. K. B. Chiappinelli, C. A. Zahnow, N. Ahuja, S. B. Baylin, Combining Epigenetic and Immunotherapy to Combat Cancer. *Cancer Research* **76**, 1683-1689 (2016).
44. M. Guo, Y. Peng, A. Gao, C. Du, J. G. Herman, Epigenetic heterogeneity in cancer. *Biomarker Research* **7**, 23 (2019).
45. Y. Chen *et al.*, Sephin1, which prolongs the integrated stress response, is a promising therapeutic for multiple sclerosis. *Brain* **142**, 344-361 (2019).
46. D. R. Leach, M. F. Krummel, J. P. Allison, Enhancement of Antitumor Immunity by CTLA-4 Blockade. *Science* **271**, 1734-1736 (1996).
47. V. P. Baklaushev *et al.*, Luciferase Expression Allows Bioluminescence Imaging But Imposes Limitations on the Orthotopic Mouse (4T1) Model of Breast Cancer. *Scientific Reports* **7**, 7715 (2017).
48. K. Wang, C. A. Phillips, A. M. Saxton, M. A. Langston, EntropyExplorer: an R package for computing and comparing differential Shannon entropy, differential coefficient of variation and differential expression. *BMC Research Notes* **8**, 832 (2015).
49. Y. Akimov, D. Bulanova, S. Timonen, K. Wennerberg, T. Aittokallio, Improved detection of differentially represented DNA barcodes for high-throughput clonal phenomics. *Molecular Systems Biology* **16**, e9195 (2020).
50. A. Dobin *et al.*, STAR: ultrafast universal RNA-seq aligner. *Bioinformatics* **29**, 15-21 (2012).
51. B. Li, C. N. Dewey, RSEM: accurate transcript quantification from RNA-Seq data with or without a reference genome. *BMC Bioinformatics* **12**, 323 (2011).
52. M. D. Robinson, D. J. McCarthy, G. K. Smyth, edgeR: a Bioconductor package for differential expression analysis of digital gene expression data. *Bioinformatics* **26**, 139-140 (2009).
53. S. Durinck, P. T. Spellman, E. Birney, W. Huber, Mapping identifiers for the integration of genomic datasets with the R/Bioconductor package biomaRt. *Nature Protocols* **4**, 1184-1191 (2009).
54. G. Klambauer *et al.*, cn.MOPS: mixture of Poissons for discovering copy number variations in next-generation sequencing data with a low false discovery rate. *Nucleic Acids Research* **40**, e69-e69 (2012).

Figure legends:

Fig 1: Experimental workflow schematic. Barcode library is introduced into mammary carcinoma cell lines *in vitro* at a low multiplicity of infection (MOI). Cells are sorted based on RFP expression to select for those that have incorporated a barcode. Barcoded cells are then transplanted into the mammary fat pad. Following immunoselection either with the endogenous immune system or immunotherapy then barcode abundance and diversity are analysed within the primary tumours and metastatic lungs.

Fig 2: Immune selection and clonal immunoediting of EMT6 primary tumours.
A. Outline of experimental design. B. EMT6 primary tumour growth plotted as tumour volume comparing wild-type Balb/c mice with immunocompromised NSG mice. Average volume +/- SEM; n=5-6 mice per group. C. Kaplan-Meier survival analysis comparing Balb/c and NSG EMT6 tumour bearing mice (Mantel-Cox p=0.009). D. EMT6 primary tumour growth plotted as tumour volume comparing

910 wild-type Balb/c mice with or without immunotherapy (anti-PD1+anti-CTLA4) IP
911 on days 10, 12, 14, and 17 indicated with red arrows. Average volume +/- SEM;
912 n=5-6 mice. E. Kaplan-Meier survival analysis comparing immunotherapy treated
913 and isotype control treated Balb/c EMT6 tumour bearing mice (Mantel-Cox
914 p=0.0006). F. Number of unique barcodes identified in EMT6 primary tumours
915 grown in NSG mice, and Balb/c mice treated with isotype control antibodies or
916 anti-PD1 + anti-CTLA4. Unpaired t-test. G. Shannon diversity index analysis
917 comparing NSG mice with Balb/c mice treated with isotype control antibodies or
918 anti-PD1 + anti-CTLA4. Unpaired t-test. H. Dot plot of a subset of barcodes with
919 interesting patterns of enrichment.
920
921 Fig 3: Immune selection and clonal immunoediting in the metastatic setting
922 utilising the 4T1 model.
923 A. Outline of experimental design. B. Kaplan-Meier survival analysis comparing
924 Balb/c and NSG 4T1 tumour bearing mice; n=5 mice/group (p = 0.0002, Mantel-
925 Cox Log-rank test). C. Kaplan-Meier survival analysis comparing immunotherapy
926 treated and isotype control treated Balb/c 4T1 tumour bearing mice. IP on days
927 15, 17, 19, and 21 indicated with red arrows; n=5-6 mice/group (p = 0.0141,
928 Mantel-Cox Log-rank test). D. Number of unique barcodes identified in 4T1
929 primary tumours and lung metastases grown in NSG mice or Balb/c mice.
930 Unpaired t-test. E. Number of unique barcodes identified in 4T1 primary tumours
931 and lung metastases grown in Balb/c mice treated with isotype control antibodies
932 or anti-PD1 + anti-CTLA4. Unpaired t-test. F. Shannon diversity index analysis
933 comparing primary tumours from NSG mice with Balb/c mice and lung metastases
934 from NSG mice, Balb/c mice, isotype control treated Balb/c mice, and anti-PD1 +
935 anti-CTLA4 treated Balb/c mice. Unpaired t-test. G. Analysis of number of unique
936 barcodes in the metastatic lungs of mice treated with control antibodies, or anti-
937 CD8a, or anti-asialo GM1. CD8 T cells depleted with anti-CD8a, NK cells depleted
938 with anti-asialo GM1. Unpaired t-test, 5 mice/group.
939
940 Fig 4: Analysis of specific barcodes enriched or depleted by the immune system
941 and immunotherapy in the 4T1 model.
942 A. Unsupervised hierarchical clustering heatmap of barcodes with an abundance
943 of above 5% in at least one 4T1 primary tumour or lung metastatic sample; *
944 indicate barcodes detected at a frequency above 0.1% in a particular sample. B.
945 Dot plot of a subset of specific barcodes. C. Fishplot of the nine most abundant
946 barcodes detected in lungs of WT and NSG mice each barcode is given a unique
947 colour with the remaining barcodes being combined and being represented in
948 grey. D. Fishplot of the nine most abundant barcodes detected in the lungs of WT
949 mice treated with combination immunotherapy or control antibodies, a
950 bottleneck has been introduced between primary tumour and lung metastases to
951 depict transition through the blood stream.
952
953 Fig 5: Gene expression analysis of immunotherapy resistant clones.
954 A. Volcano plot showing differentially expressed genes between parental 4T1 cells
955 and the immunotherapy enriched 1 (IE1) clone. B. Volcano plot showing
956 differentially expressed genes between parental 4T1 cells and the immunotherapy
957 enriched 2 (IE2) clone. C. Expression of MHC related genes co-ordinately down-
958 regulated in clone IE1, measured as transcripts per million (TPM) in the parental

4T1 population and in the specific cell clones; unpaired t-test. D. MHC1 protein expression as quantified by flow cytometry in the specific clones and the parental 4T1 population measured as mean fluorescence intensity (MFI); representative histogram showing each immune enriched clone and the parental cells on the right; unpaired t-test. E. Expression of immune related genes up-regulated in clone IE2, measured as transcripts per million (TPM) in the parental 4T1 population and in the specific cell clones; unpaired t-test. F. PD-L1 protein expression as determined by flow cytometry in the specific clones and the parental 4T1 population measured as mean fluorescence intensity (MFI), representative plot of three independent experiments; unpaired t-test.

Fig 6. Overlapping gene signatures of the immunotherapy resistant clones show prognostic significance in basal-like breast cancer patients.
A. Upset plots and Venn diagrams showing the overlap in significantly up-regulated (right) and down-regulated (left) genes between the two immunotherapy enriched clones and two other control clones. B. Heatmap of the top 50 overlapping up regulated and down regulated genes between the IE1 and IE2 clones across all the clonal cell lines. C. Kaplan-Meier survival analysis of basal-like breast cancer patients from the METABRIC cohort, examining overall survival with patients split based on the top 30% and bottom 30% expression of the overlapping upregulated 25 gene signature. D. Kaplan-Meier survival analysis of basal-like breast cancer patients from the TCGA cohort, examining overall survival with patients split based on the top 30% and bottom 30% expression of the overlapping upregulated 25 gene signature. The Cox proportional hazards model was used to compute Hazard Ratios. Significance between stratification groups were computed using log-rank test statistics.

Supplementary Figure Legends:

Sup Fig1. 4T1 primary tumour growth or barcode diversity unchanged in immunocompromised mice. A. Primary tumour mass was slightly increased in immunocompromised NSG mice. B. Total number of unique barcodes identified in the primary tumours of Balb/c or NSG mice. C. Shannon diversity analysis comparing primary tumours from Balb/c and NSG mice.

Sup Fig2. Depletion of CD8+ T cells or NK cells does not significantly affect survival in 4T1 tumour bearing mice. CD8 T cells depleted with anti-CD8a, NK cells depleted with anti-asialo GM1. A. Kaplan-Meier survival analysis of Balb/c mice transplanted with 4T1 cells, primary tumour was resected on day 15. Cell depletion was initiated 1 day prior to resection on day 14.

Sup Fig3. Analysis of higher complexity barcode library in the 4T1 cells replicates changes in barcode proportions that were seen in the ~5000 barcode library. A. Number of unique barcodes identified in 4T1 primary tumours and lung metastases grown in NSG mice or Balb/c mice. Unpaired t-test. 5 mice/group. B. Number of unique barcodes identified in 4T1 primary tumours and lung metastases grown in Balb/c mice treated with isotype control antibodies or anti-PD1 + anti-CTLA4. Unpaired t-test. 5 mice/group.

1007 Sup Fig 4. 4T1 clonal cell lines growth kinetics *in vitro*. Growth kinetics as
1008 measured by percentage confluence over time.
1009
1010 Sup Fig 5. A. No genomic loss was observed in any of the clones at the MHC-I locus
1011 on chromosome 17. B. Gene expression changes in genes that have a single copy
1012 number increase were observed in IE1 and IE2 but not NT2.
1013
1014
1015 Sup Fig 6. MHC regulation by 5-aza and IFN-γ in the clonal cell lines. A. 5-aza
1016 treatment of clonal cell lines increases MHC-I protein expression in a dose
1017 dependent manner in all cell lines as measured by flow cytometry. Unpaired t-
1018 test. B. IFN-γ treatment of clonal cell lines increases MHC-I protein expression in
1019 all cell lines.
1020
1021 Sup Fig 7. Gene set enrichment analysis of the overlapping genes between the IE1
1022 and IE2 clones. Red indicates gene sets with a significant
1023
1024 **Supplementary Table Legends:**
1025 Sup Table 1: DNA barcode insertion sites of IE1 and IE2. By searching the whole
1026 genome sequencing (WGS) data and identifying read pairs where only one read
1027 mapped to the barcode sequence, the matching mate was blasted against mm10
1028 to identify the barcode plasmid insertion site. Both barcodes were found to reside
1029 in introns of cancer-related genes but there was no difference in expression of
1030 these genes detected.
1031
1032 Sup Table 2: Copy number variation (CNV) locations found within all subclones.
1033 By analysing whole genome sequencing data in R using the cn.mops pacakges,
1034 copy number variations could be determined. No major copy number aberrations
1035 were detected across the clones, although a single copy number gain was detected
1036 in IE1, IE2 and NT2.
1037
1038 Sup Table 3. List of genes differentially expressed in IE1 compared to parental 4T1
1039 bulk. Differentially expressed genes (DEGs) were generated by analyzing bulk
1040 RNA sequencing data using R and the EdgeR package. DEGs were filtered for
1041 significance based on a FDR <0.05.
1042
1043 Sup Table 4. List of genes differentially expressed in IE2 compared to parental 4T1
1044 bulk. Differentially expressed genes (DEGs) were generated by analyzing bulk
1045 RNA sequencing data using R and the EdgeR package. DEGs were filtered for
1046 significance based on a FDR <0.05. A greater number of differentially expressed
1047 genes were detected in IE2 than IE1.
1048
1049 Sup Table 5. All significantly enriched gene sets found in IE1. Differentially
1050 expressed genes generated from comparing IE1 to bulk were preranked by fold
1051 change before searching for gene set enrichment using the Molecular Signature
1052 Database (MSigDB) across all available collections. Gene sets were filtered for
1053 significance based on a FDR<0.05.
1054

1055 Sup Table 6. All significantly enriched gene sets found in IE2. Differentially
1056 expressed genes generated from comparing IE2 to bulk were preranked by fold
1057 change. Gene set enrichment was carried out using Molecular Signature Database
1058 (MSigDB) across all available collections. Gene sets were filtered for significance
1059 based on a FDR<0.05
1060
1061 Sup Table 7: List of common differentially expressed genes found in IE1 and IE2.
1062 Commonly differentially expressed genes (DEGs) were determined by
1063 overlapping significant DEGs in IE1 and IE2 by gene name. An average fold change
1064 was calculated across the two samples.
1065
1066 Sup Table 8: Top significantly enriched gene sets found from common
1067 differentially expressed genes in IE1 and IE2. The fold change of the common
1068 differentially expressed genes in IE1 and IE2 were averaged together to generate
1069 an average fold change across both IE1 and IE2. The gene list was then preranked
1070 before searching for gene set enrichment using Molecular Signature Database
1071 (MSigDB) across the C2 All collection. Gene sets were filtered for significance
1072 based on a FDR<0.05. The majority of significant gene sets that were returned
1073 were negatively enriched in IE1 and IE2.
1074
1075

Figure 1

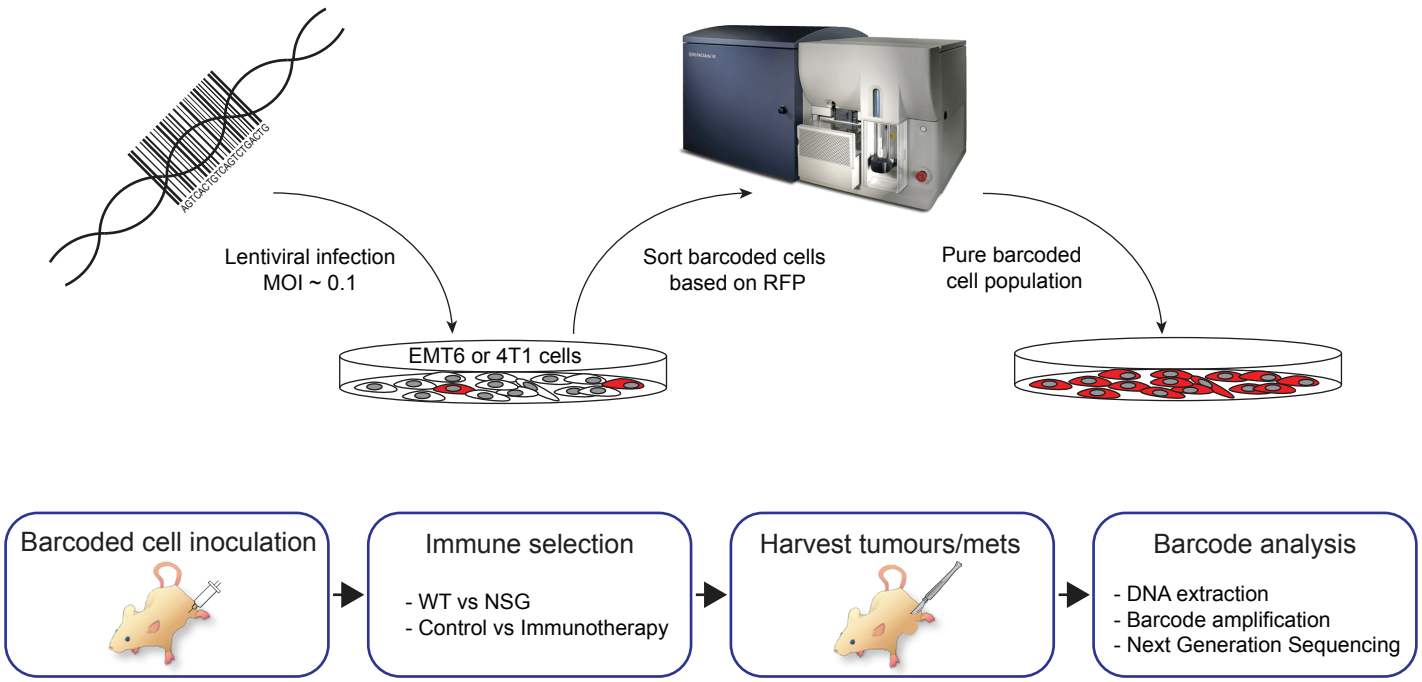
AGTCACTGTCAGTCTGACTG
Lentiviral infection
MOI ~ 0.1
EMT6 or 4T1 cells
Sort barcoded cells
based on RFP
Pure barcoded
cell population
Barcoded cell inoculation
Immune selection
- WT vs NSG
- Control vs Immunotherapy
Harvest tumours/mets
Barcode analysis
- DNA extraction
- Barcode amplification
- Next Generation Sequencing

Figure 2

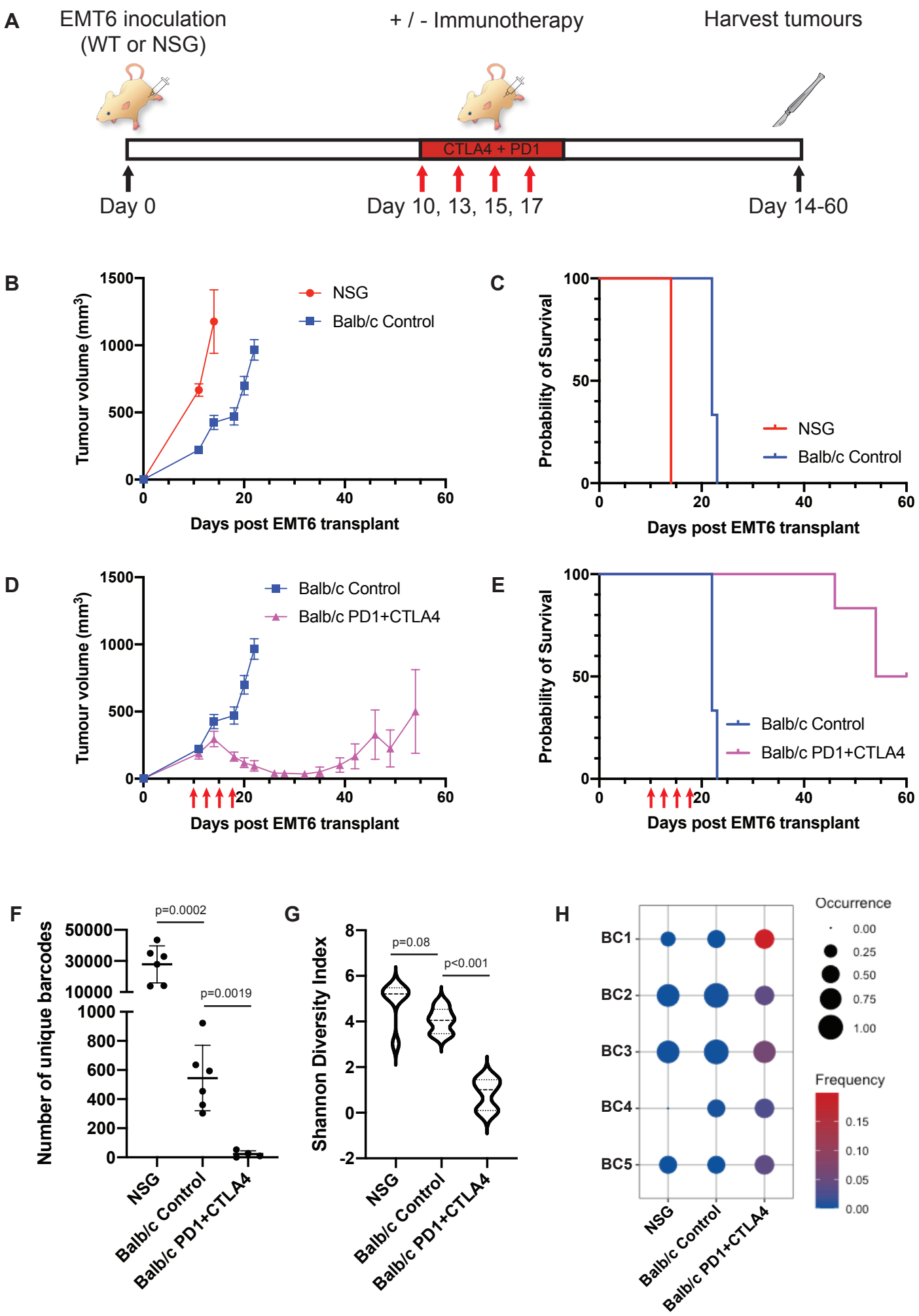
A
EMT6 inoculation
(WT or NSG)
+ / - Immunotherapy
Harvest tumours
CTLA4 + PD1
Day 0
Day 10, 13, 15, 17
Day 14-60
B
Tumour volume (mm³)
Days post EMT6 transplant
NSG
Balb/c Control
C
Probability of Survival
Days post EMT6 transplant
NSG
Balb/c Control
D
Tumour volume (mm³)
Days post EMT6 transplant
Balb/c Control
Balb/c PD1+CTLA4
E
Probability of Survival
Days post EMT6 transplant
Balb/c Control
Balb/c PD1+CTLA4
F
Number of unique barcodes
p=0.0002
p=0.0019
NSG
Balb/c Control
Balb/c PD1+CTLA4
G
Shannon Diversity Index
p=0.08
p<0.001
NSG
Balb/c Control
Balb/c PD1+CTLA4
H
BC1
BC2
BC3
BC4
BC5
NSG
Balb/c Control
Balb/c PD1+CTLA4
Occurrence
0.00
0.25
0.50
0.75
1.00
Frequency
0.15
0.10
0.05
0.00

Figure 3

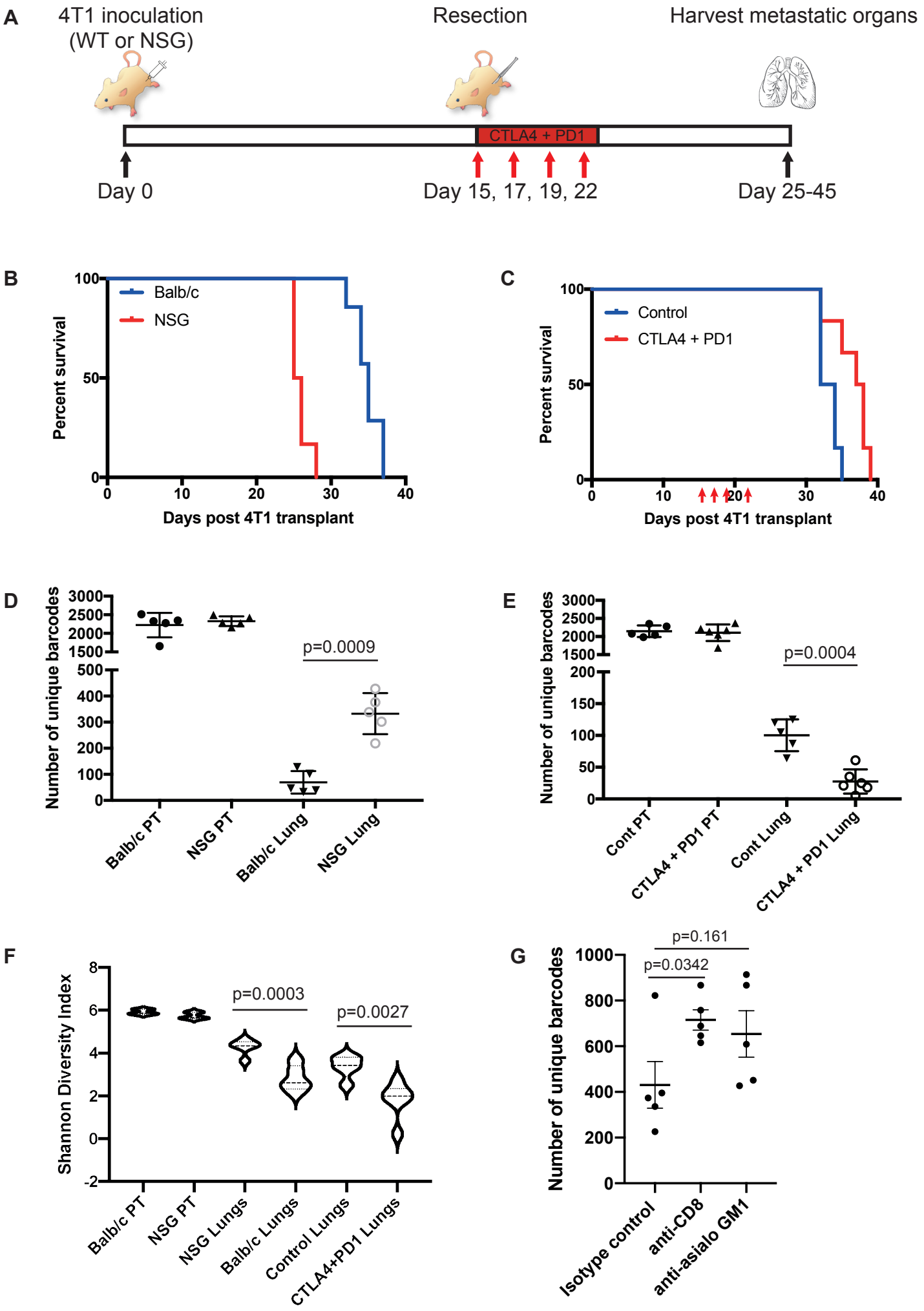
A
4T1 inoculation
(WT or NSG)
Resection
Harvest metastatic organs
CTLA4 + PD1
Day 0
Day 15, 17, 19, 22
Day 25-45
B
Balb/c
NSG
Percent survival
Days post 4T1 transplant
C
Control
CTLA4 + PD1
Percent survival
Days post 4T1 transplant
D
Number of unique barcodes
p=0.0009
Balb/c PT
NSG PT
Balb/c Lung
NSG Lung
E
Number of unique barcodes
p=0.0004
Cont PT
CTLA4 + PD1 PT
Cont Lung
CTLA4 + PD1 Lung
F
Shannon Diversity Index
p=0.0003
p=0.0027
Balb/c PT
NSG PT
NSG Lungs
Balb/c Lungs
Control Lungs
CTLA4+PD1 Lungs
G
Number of unique barcodes
p=0.161
p=0.0342
Isotype control
anti-CD8
anti-asialo GM1

Figure 4

A

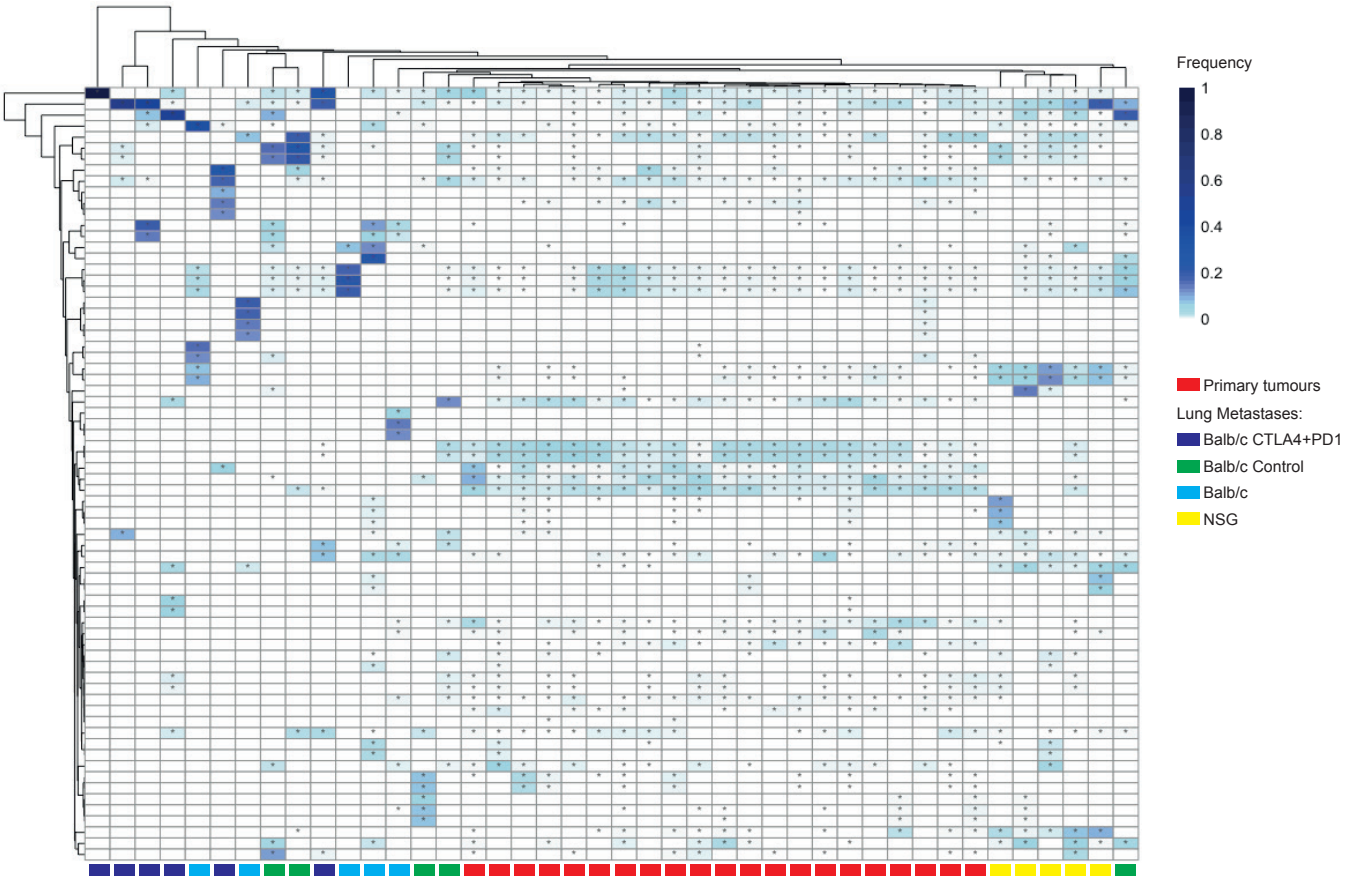

B

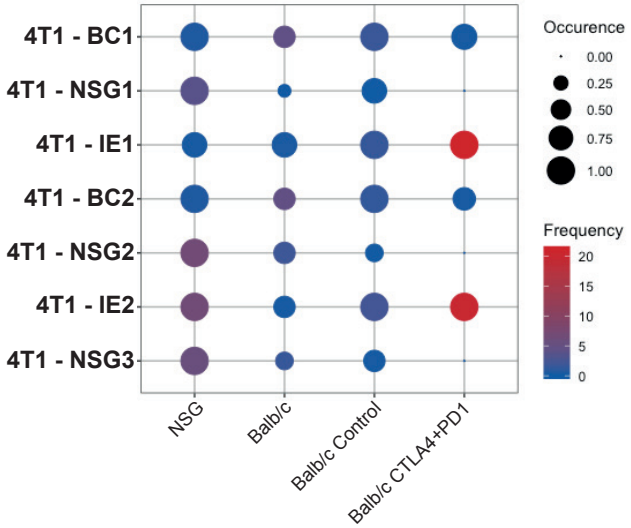

C

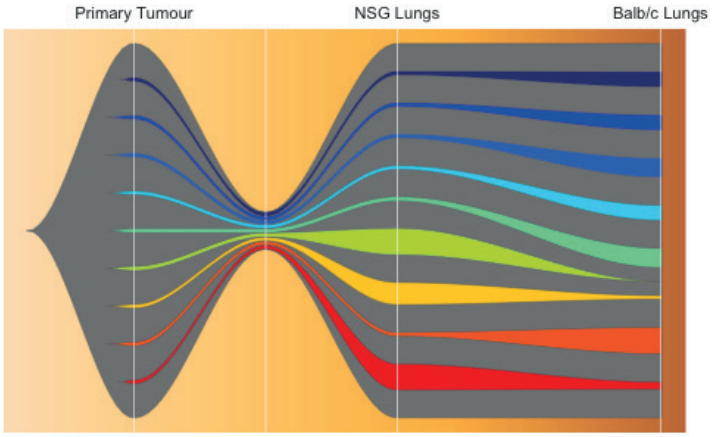

D

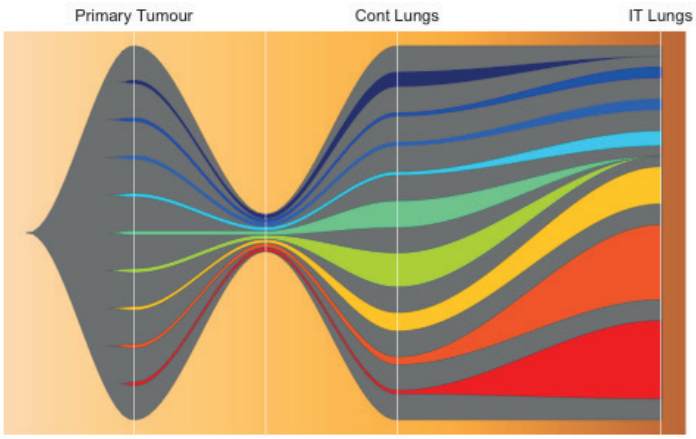

Figure 5

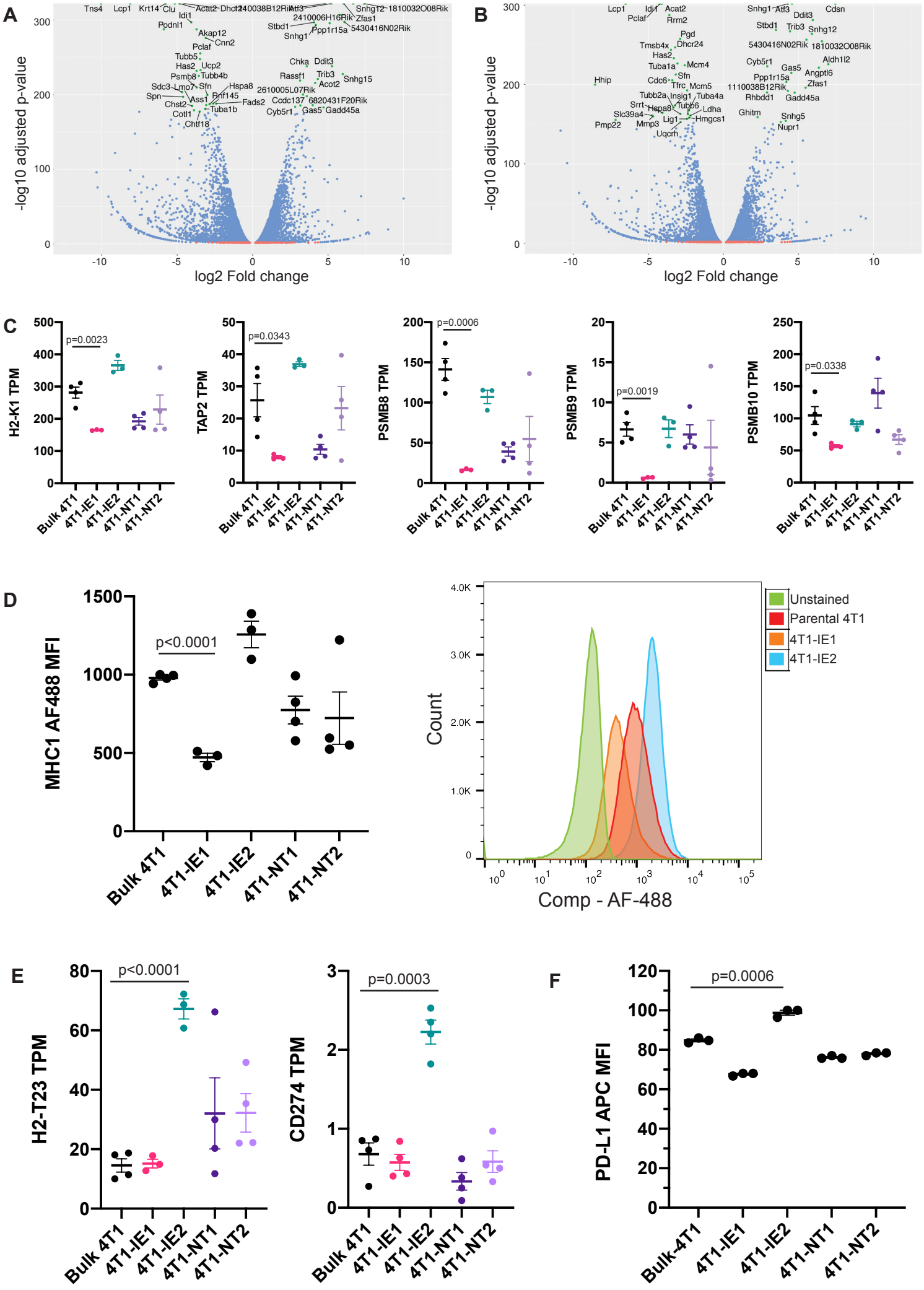
A
-log10 adjusted p-value
log2 Fold change
B
-log10 adjusted p-value
log2 Fold change
C
H2-K1 TPM
p=0.0023
TAP2 TPM
p=0.0343
PSMB8 TPM
p=0.0006
PSMB9 TPM
p=0.0019
PSMB10 TPM
p=0.0338
Bulk 4T1
4T1-IE1
4T1-IE2
4T1-NT1
4T1-NT2
D
MHC1 AF488 MFI
p<0.0001
Bulk 4T1
4T1-IE1
4T1-IE2
4T1-NT1
4T1-NT2
Count
Comp - AF-488
Unstained
Parental 4T1
4T1-IE1
4T1-IE2
E
H2-T23 TPM
p<0.0001
CD274 TPM
p=0.0003
Bulk 4T1
4T1-IE1
4T1-IE2
4T1-NT1
4T1-NT2
F
PD-L1 APC MFI
p=0.0006
Bulk-4T1
4T1-IE1
4T1-IE2
4T1-NT1
4T1-NT2

Figure 6

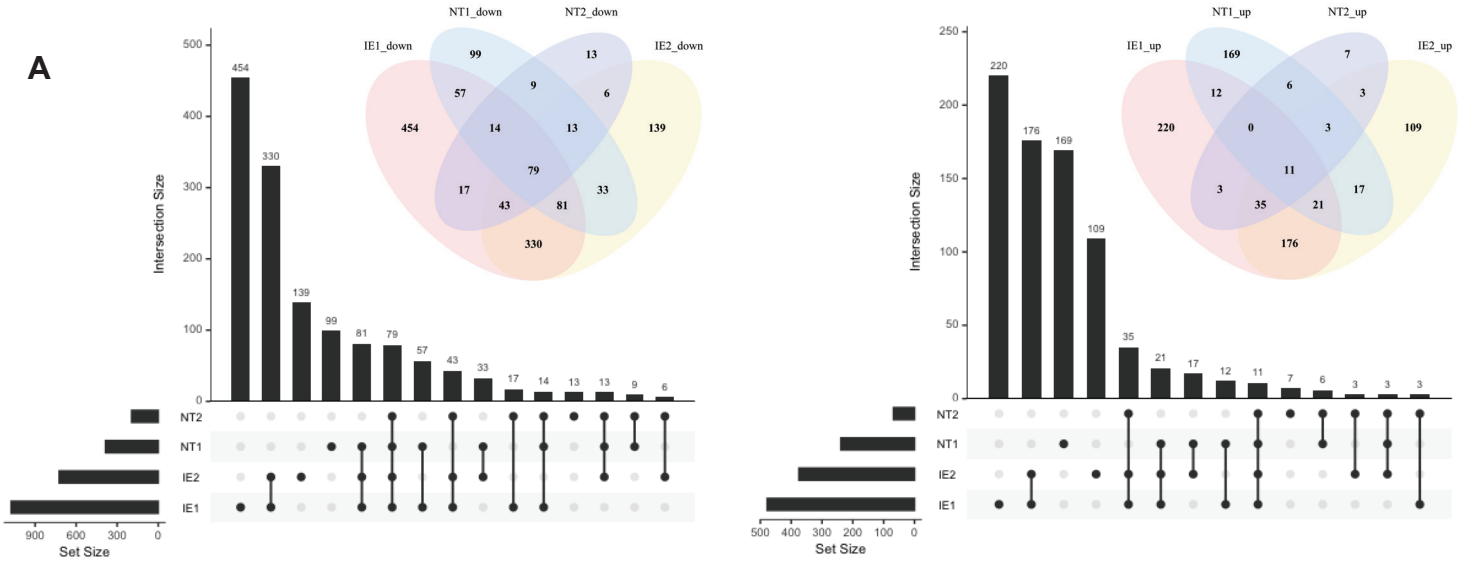
A
NT1_down
NT2_down
IE1_down
IE2_down
Intersection Size
Set Size
NT2
NT1
IE2
IE1
NT1_up
NT2_up
IE1_up
IE2_up

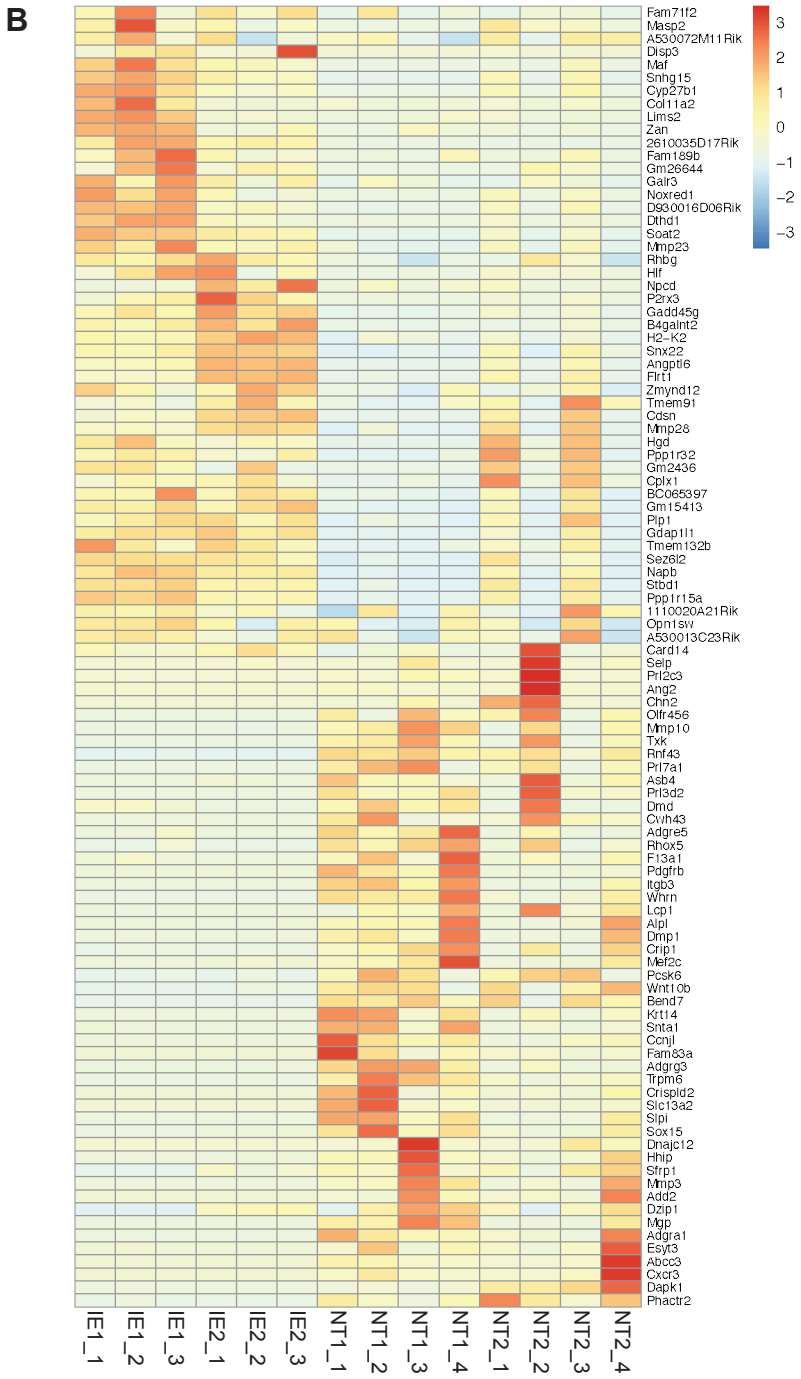
B
IE1_1
IE1_2
IE1_3
IE2_1
IE2_2
IE2_3
NT1_1
NT1_2
NT1_3
NT1_4
NT2_1
NT2_2
NT2_3
NT2_4

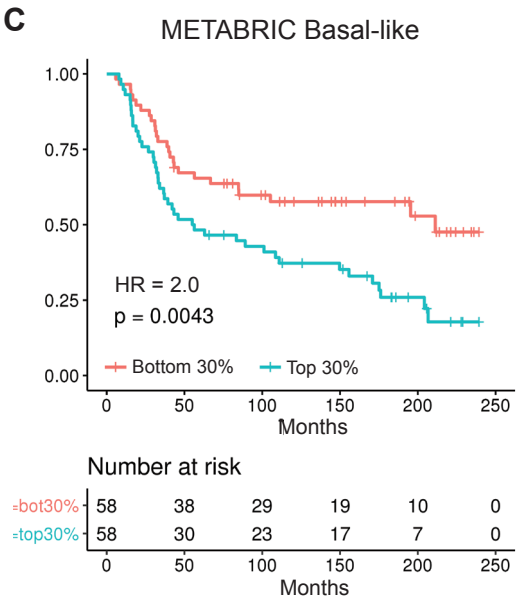
C
METABRIC Basal-like
HR = 2.0
p = 0.0043
Bottom 30%
Top 30%
Months
Number at risk
=bot30% 58 38 29 19 10 0
=top30% 58 30 23 17 7 0

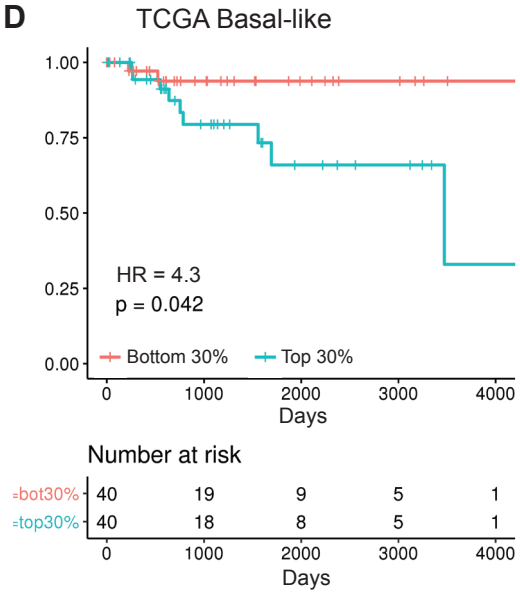
D
TCGA Basal-like
HR = 4.3
p = 0.042
Bottom 30%
Top 30%
Days
Number at risk
=bot30% 40 19 9 5 1
=top30% 40 18 8 5 1

Sup Figure 1

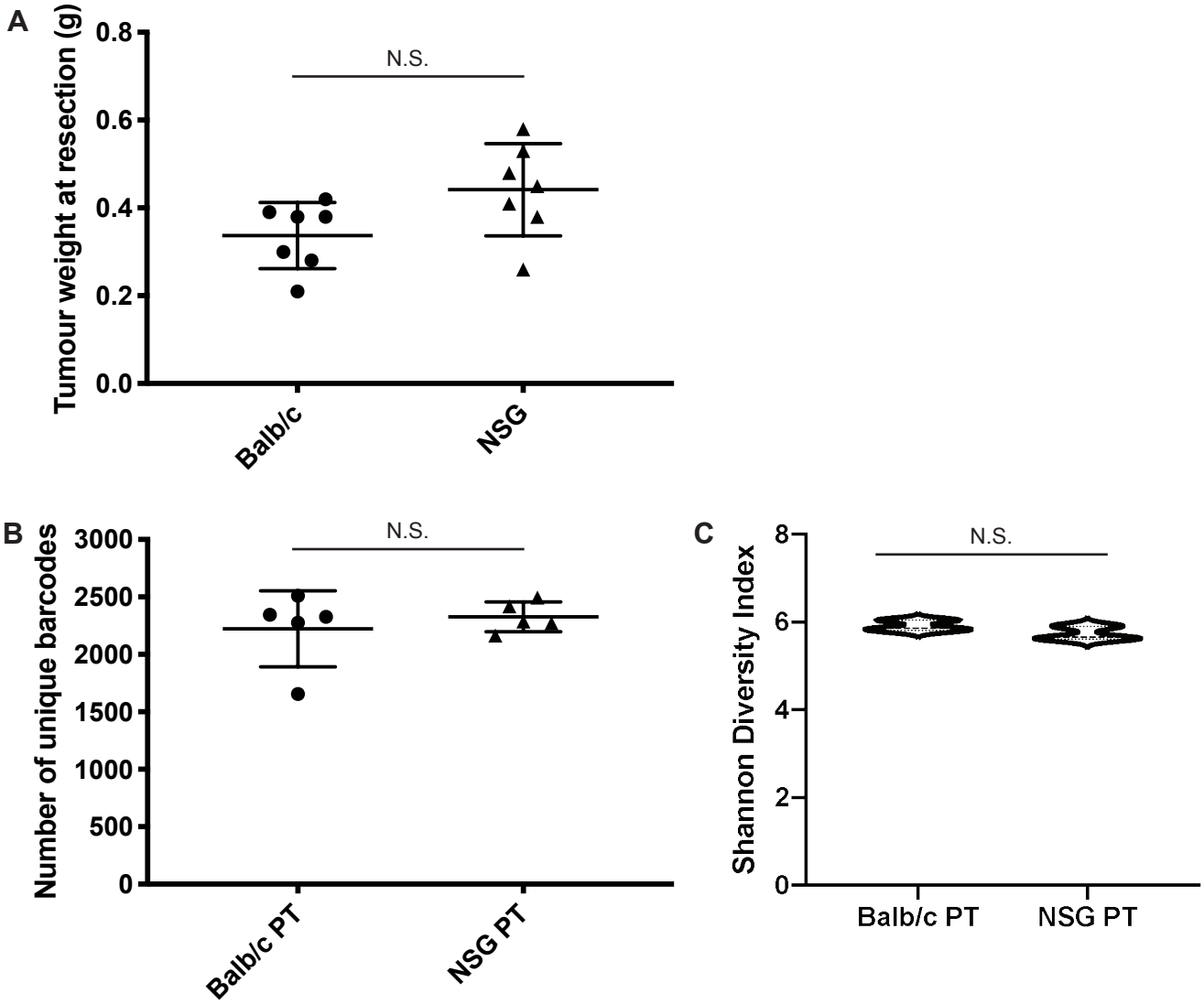
A
Tumour weight at resection (g)
0.8
0.6
0.4
0.2
0.0
N.S.
Balb/c
NSG
B
Number of unique barcodes
3000
2500
2000
1500
1000
500
0
N.S.
Balb/c PT
NSG PT
C
Shannon Diversity Index
8
6
4
2
0
N.S.
Balb/c PT
NSG PT

Sup Figure 3

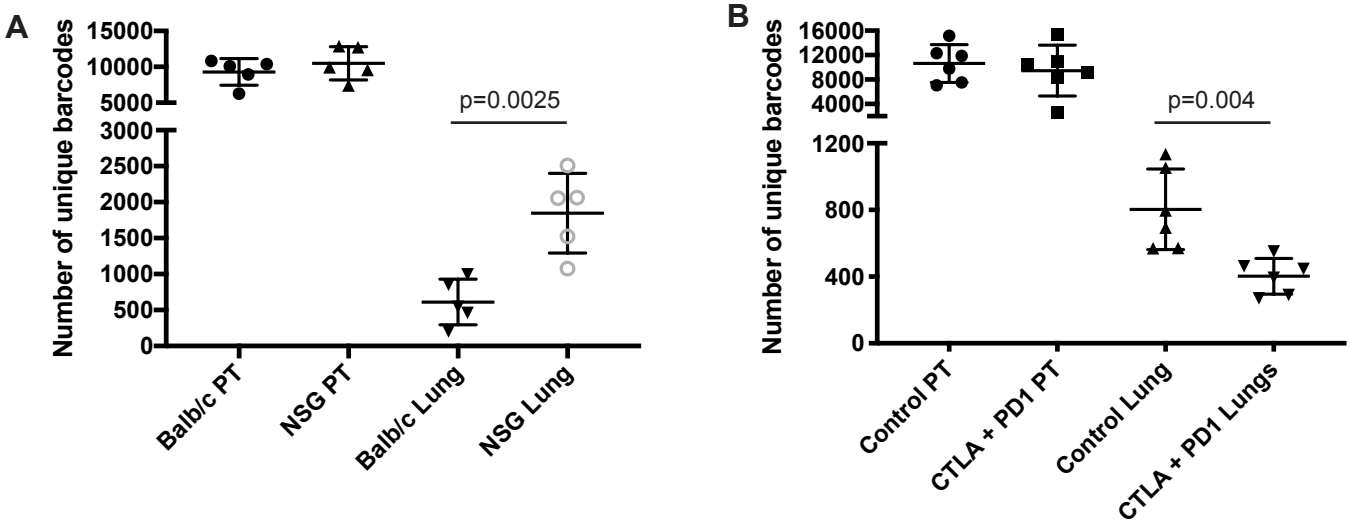
A
Number of unique barcodes
15000
10000
5000
3000
2500
2000
1500
1000
500
0
p=0.0025
Balb/c PT
NSG PT
Balb/c Lung
NSG Lung
B
Number of unique barcodes
16000
12000
8000
4000
1200
800
400
0
p=0.004
Control PT
CTLA + PD1 PT
Control Lung
CTLA + PD1 Lungs

Sup Figure 4

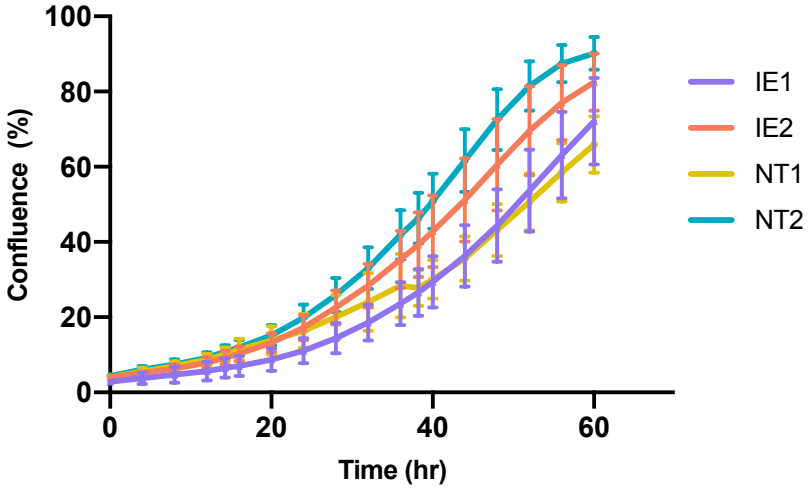

Sup Figure 5

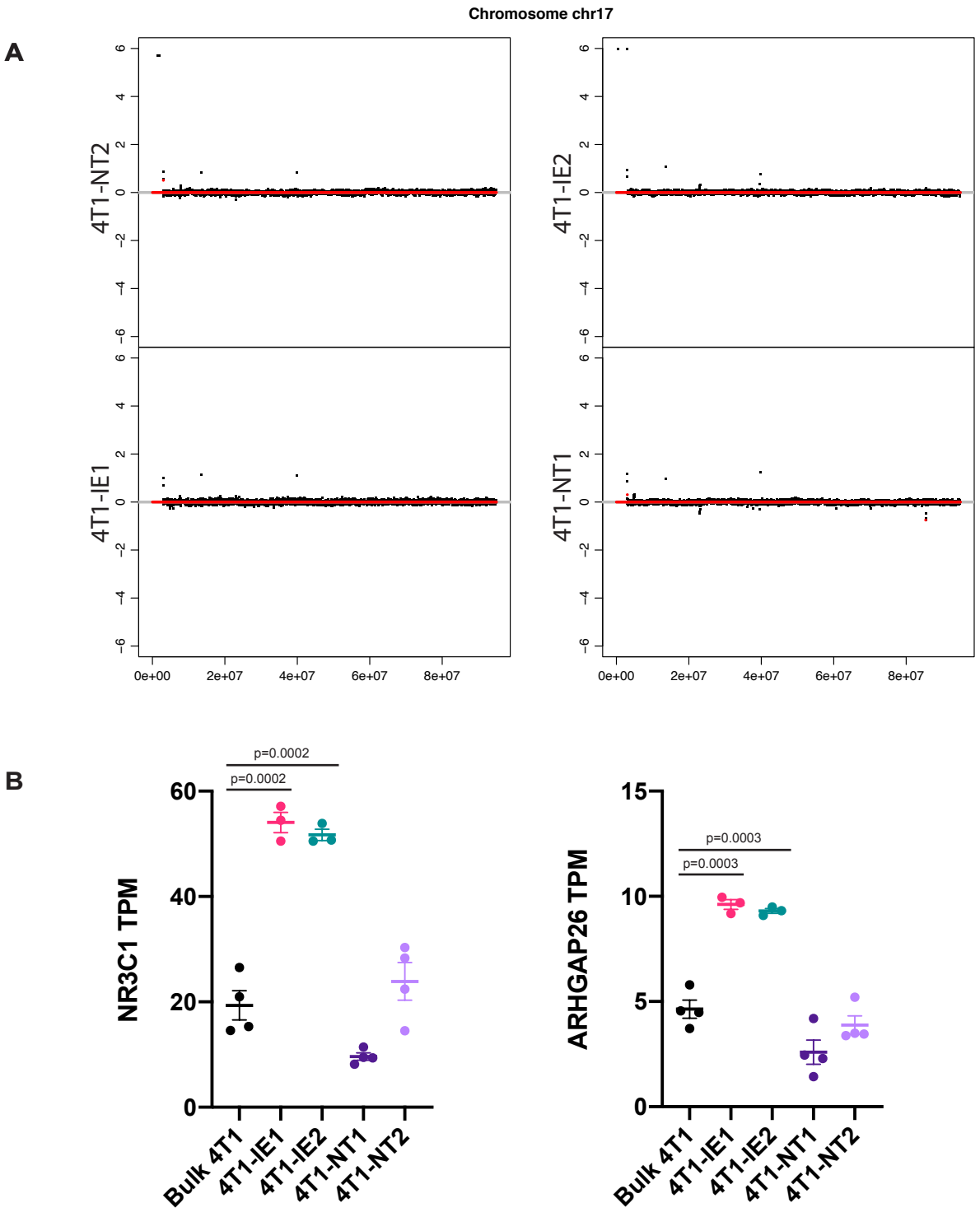
A
Chromosome chr17
4T1-NT2
4T1-IE2
4T1-IE1
4T1-NT1
6
4
2
0
−2
−4
−6
0e+00
2e+07
4e+07
6e+07
8e+07
B
p=0.0002
p=0.0002
NR3C1 TPM
60
40
20
0
Bulk 4T1
4T1-IE1
4T1-IE2
4T1-NT1
4T1-NT2
p=0.0003
p=0.0003
ARHGAP26 TPM
15
10
5
0

Sup Figure 6

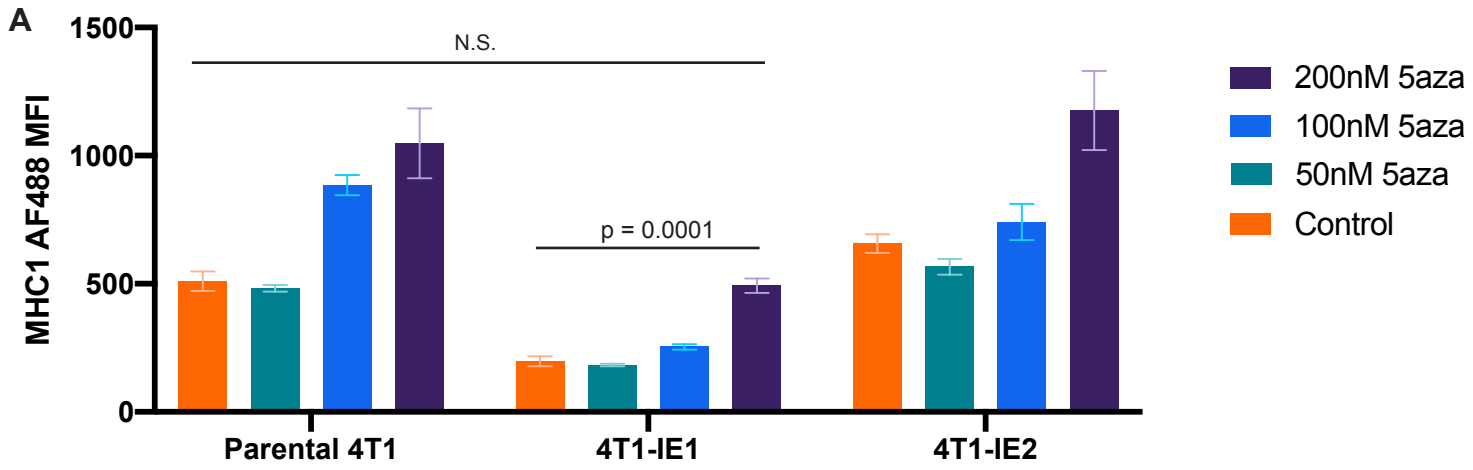
A
1500
1000
500
0
MHC1 AF488 MFI
N.S.
p = 0.0001
Parental 4T1
4T1-IE1
4T1-IE2
200nM 5aza
100nM 5aza
50nM 5aza
Control

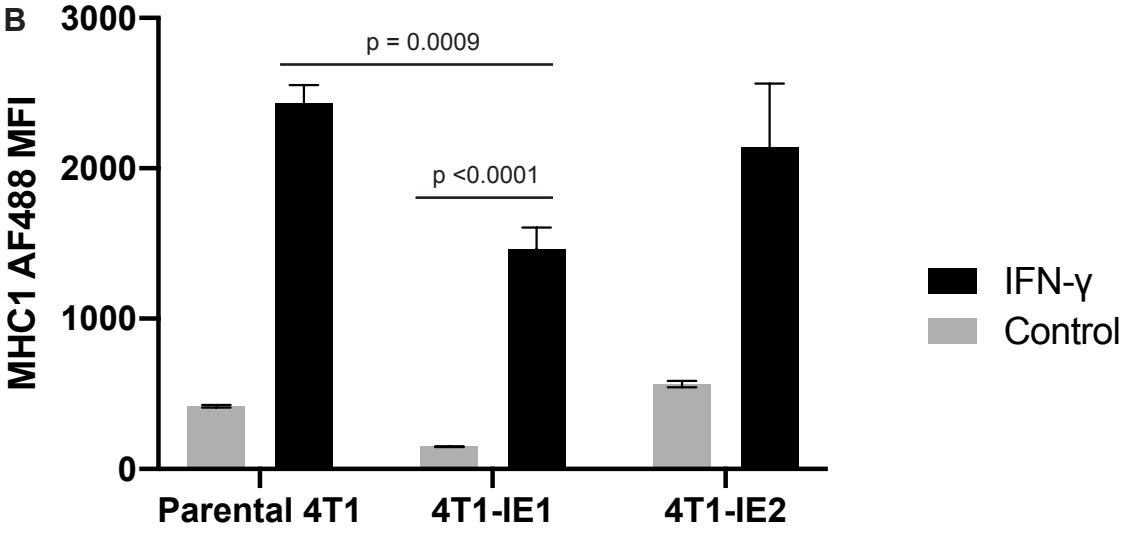
B
3000
2000
1000
0
MHC1 AF488 MFI
p = 0.0009
p <0.0001
Parental 4T1
4T1-IE1
4T1-IE2
IFN-γ
Control

Sup Figure 7

A

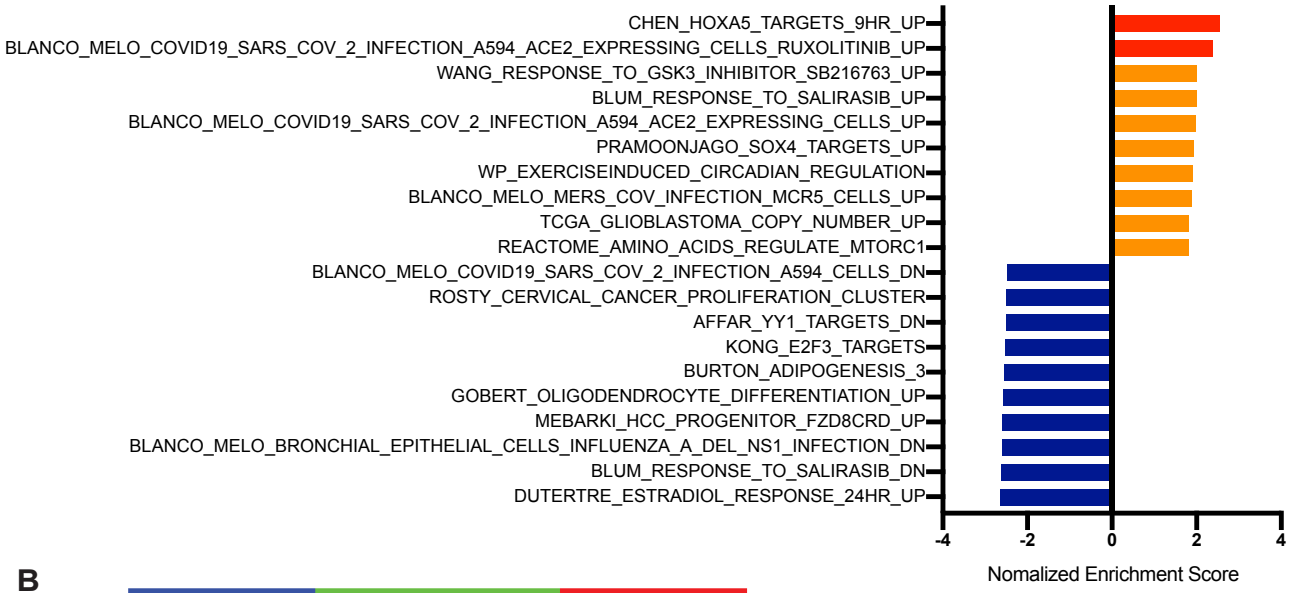

B

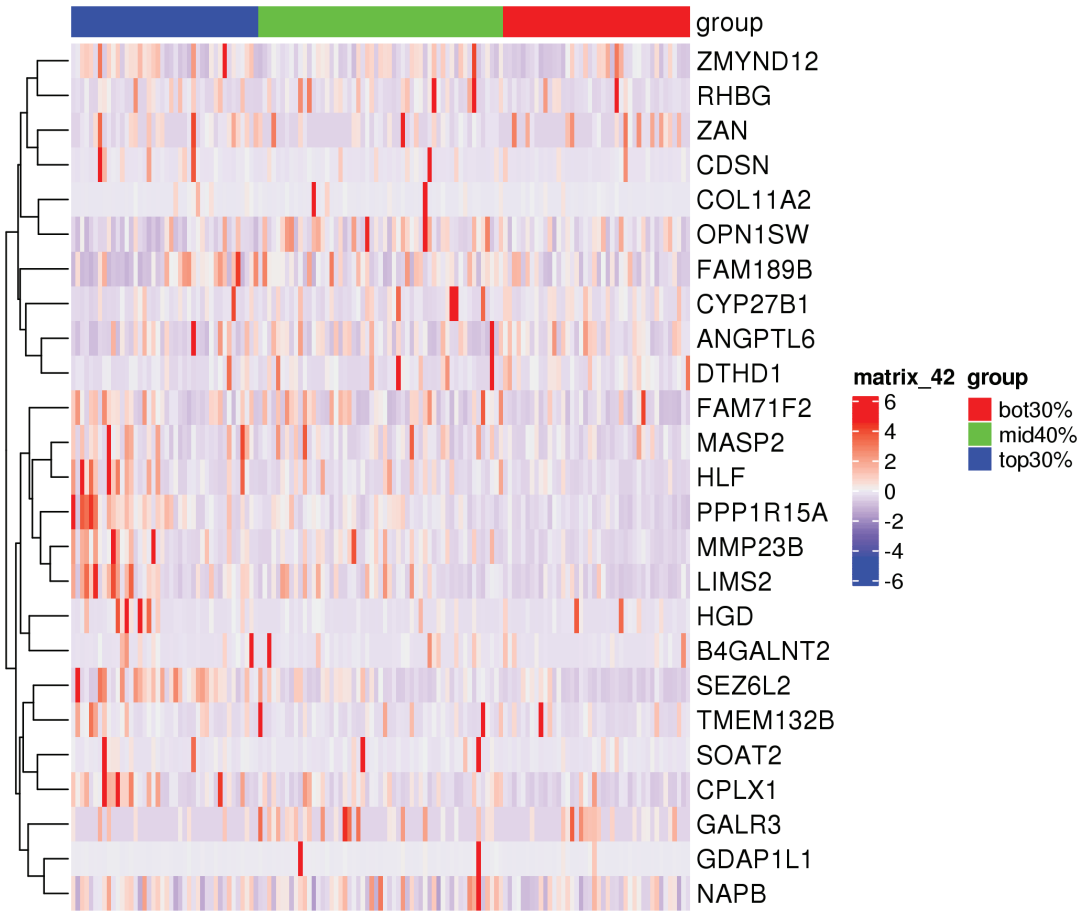

C

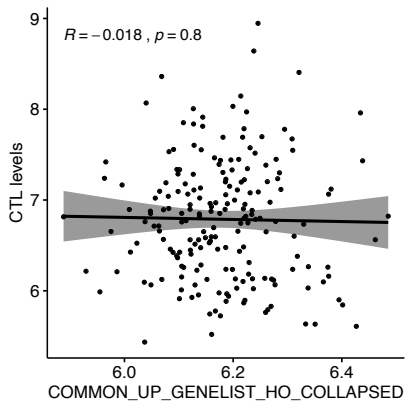
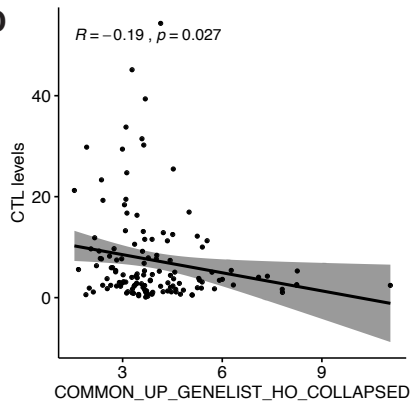
D